SAND REPORT

SAND2002-2175
Unlimited Release
Printed July 2002

Towards Numerical Simulation of Shock Induced Combustion Using Probability Density Function Approaches

Paul E. DesJardin, Mel R. Baer, Raymond L. Bell, and Eugene S. Hertel

Prepared by
Sandia National Laboratories
Albuquerque, New Mexico 87185 and Livermore, California 94550

Sandia is a multiprogram laboratory operated by Sandia Corporation, a Lockheed Martin Company, for the United States Department of Energy under Contract DE-AC04-94AL85000.

Sandia National Laboratories

Issued by Sandia National Laboratories, operated for the United States Department of Energy by Sandia Corporation.

Available to DOE and DOE contractors from
U.S. Department of Energy
Office of Scientific and Technical Information
P.O. Box 62
Oak Ridge, TN 37831

Telephone: (865)576-8401
Facsimile: (865)576-5728
E-Mail: reports@adonis.osti.gov
Online ordering: http://www.doe.gov/bridge

Available to the public from
U.S. Department of Commerce
National Technical Information Service
5285 Port Royal Rd
Springfield, VA 22161

Telephone: (800)553-6847
Facsimile: (703)605-6900
E-Mail: orders@ntis.fedworld.gov
Online order: http://www.ntis.gov/ordering.htm

SAND2002-2175
Unlimited Release
Printed July, 2002

Towards Numerical Simulation of Shock Induced Combustion Using Probability Density Function Approaches

Paul E. DesJardin
Fire Science and Technology

Mel R. Baer and Eugene S. Hertel
Thermal and Reactive Processes

Raymond L. Bell
Computational Physics and Simulation Frameworks

Sandia National Laboratories
P.O. Box 5800
Albuquerque, New Mexico 87185-1135

Abstract

The specific problem to be addressed in this work is the secondary combustion that arises from shock-induced mixing in volumetric explosives. It has been recognized that the effects of combustion due to secondary mixing can greatly alter the expansion of gases and dispersal of high-energy explosive. Furthermore, this enhanced effect may be a tailored feature for the new energetic material systems. One approach for studying this problem is based on the use of Large Eddy Simulation (LES) techniques. In this approach, the large turbulent length scales of motion are simulated directly while the small scales of turbulent motion are explicitly treated using a subgrid scale (SGS) model. The focus of this effort is to develop a SGS model for combustion that is applicable to shock-induced combustion events using probability density function (PDF) approaches. A simplified presumed PDF combustion model is formulated and implemented in the CTH shock physics code. Two classes of problems are studied using this model. The first is an isolated piece of reactive material burning with the surrounding air. The second problem is the dispersal of highly reactive material due to a shock driven explosion event. The results from these studies show the importance of incorporating a secondary combustion modeling capability and the utility of using a PDF-based description to simulate these events.

Acknowledgments

This work was supported through the senior scientist lab directed research and development (LDRD) program at Sandia National Laboratories and the reactive fragments program supported by the Naval Surface Warfare Center with Mr. Leonard Wilson serving as technical monitor. The authors gratefully acknowledge Dr. Robert Schmidt of Sandia National Laboratories for his suggestions on the coding of the models developed in this study into CTH. Sandia is a multiprogram laboratory operated by Sandia Corporation, a Lockheed Martin Company, for the United States Department of Energy under Contract DE-AC04-94AL85000.

NOMENCLATURE

Roman Symbols

C_I = Model constant for the scalar dissipation rate, $C_I = 0.07$

C_P = Specific heat at constant pressure $[J/(kg-K)]$

C_s = Model constant for the turbulent eddy viscosity, $C_s = 0.012$

C_v = Specific heat at constant volume $[J/(kg-K)]$

Den = Denominator of state-relationship

Dif = Diffusion term in σ_Z^2 transport equation $[kg/(m^3-s)]$

D_m = Molecular diffusivity $[m^2/s]$

D_p = Characteristic diameter of reactive particle $[m]$

D_T = Turbulent diffusivity $[m^2/s]$

$h_{f_i}^o$ = Heat of formation for the ith species $[J/(kg-K)]$

$I_{Z_{st}}$ = Incomplete beta function evaluated at Z_{st}

MW = Molecular weight $[kg/m^3]$

P_ϕ = Filtered probability density function for the variable ϕ

$P_{\alpha\beta\gamma\ldots}$ = Joint filtered probability density function for the variables $\alpha\beta\gamma\ldots$

S_{ij} = Strain-rate tensor $[1/s]$

$|S|$ = Magnitude of the strain-rate tensor (*i.e.* $|S| = \sqrt{2S_{ij}S_{ij}}$)$[1/s]$

Y_i = Mass fraction of the ith species

Z, ς = Mixture fraction

Greek Symbols

Δ_f = Filter width $[m]$

Δt = Time step $[s]$

Γ = Gamma function

γ = Ratio of specific heats, $\gamma = C_P/C_v$

χ = Scalar dissipation rate, $\chi = 2D_m\langle \nabla Z \bullet \nabla Z \rangle$ $[1/s]$

ν_T = Turbulent eddy viscosity $[m^2/s]$

ρ = Density $[kg/m^3]$

σ_ϕ^2 = SGS variance for the variable ϕ

ω_i''' = Reaction rate of the i^{th} species $[kg/m^3]$

ξ = Rotational degrees of freedom in EOS

Nondimensional Parameters

Sc_T = Turbulent Schmidt number, $Sc_T = 0.3$

Subscript Symbols

i = i^{th} species

st = Stoichiometric value

Abbreviations

EOS = Equation of State
FDF = Filtered Probability Density Function
JFDF = Joint Filtered Probability Density Function
LES = Large Eddy Simulation
LHF = Locally-Homogeneous Flow
MILES = Monotonically Integrated Large Eddy Simulation
PGS = Pressure Gradient Scaling
RANS = Reynolds Averaged Navier Stokes
SGS = Subgrid Scale

Mathematical Operators

$\langle \varphi \rangle$ = Filtered φ quantity, *i.e.*, $\langle \varphi \rangle = \int_\infty \varphi G dV$ where G is a filter weighting function.

$\langle \alpha | \beta \rangle$ = Conditionally filtered value of α on the variable β

Constants

π = Pi [3.14159.....]

$\Re$ = Universal gas constant, 8.3144 $kJ/kmol-K$

TABLE OF CONTENTS

LIST OF FIGURES

1. Introduction

The specific problem to be addressed in this work is the secondary combustion that arises from a shock-induced mixing event. It has been recognized that the effects of combustion due to secondary mixing can greatly alter the expansion of gases and dispersal of high-energy explosive. Figure 1.1 shows the dispersal of a mixture of reactive material from an initial high explosive event using the CTH shock physics code [1]. Hot reactive material is ejected on the order of milliseconds and begins to entrain surrounding air due to local turbulent mixing processes.

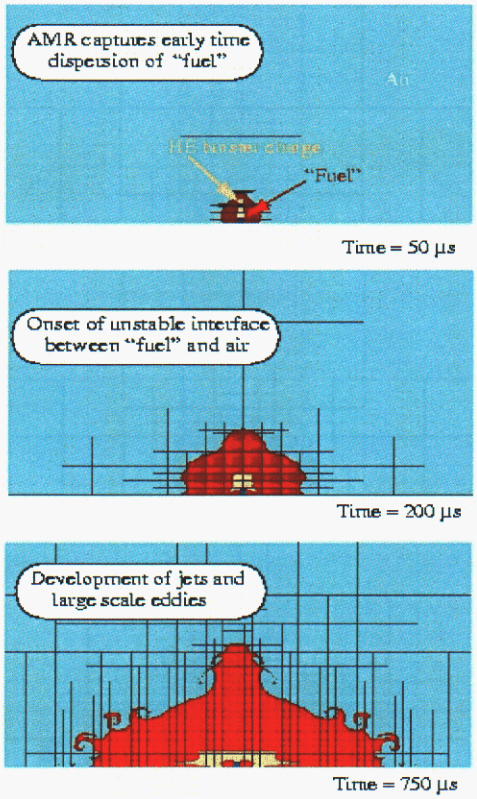

Figure 1.1: Dispersal of reactive material from an initial detonation event.

If the dispersed reactive material is at a sufficient temperature, or is ignited through other means (*e.g.* shock focusing), then enhanced impulse loading can result from secondary combustion. The modeling of this event is the focus of this work.

In recent years, remarkable progress has been made in the theory of turbulent combustion, however, much of this success is limited to simple flows such as jets and plumes. These new approaches have limited use in shock-driven flows. Numerical simulation of turbulent combustion from first principles requires resolving several decades of time and length scales that are only possible for the simplest of flow fields at low Reynolds number for which numerical simulations are often limited to 2D. Simulating 3D turbulent reacting flows of engineering interest requires the

use subgrid scale (SGS) modeling for which only the largest scales of turbulence are directly simulated while the smallest scales are modeled. The precise understanding of the secondary combustion event involving the non-linear coupling of multiphase gas-liquid-solid phase turbulent mixing, heat transfer and combustion processes is still the subject of on-going research.

The approach to addressing this problem is based on the use of Large Eddy Simulation (LES). In LES, the turbulent mixing processes are partitioned into length scales resolved using a CFD grid, and length scales that fall below the grid, requiring explicit subgrid scale (SGS) model closures. Since most of the processes associated with combustion occur at length scales that fall below the grid scale, then accounting for these effects presents a formidable challenge for SGS modeling. One method to construct SGS models of combustion is through statistical means, for which a filtered probability density function (FDF) or filtered joint probability density function (JFDF) of composition and temperature is either assumed or explicitly determined using Monte Carlo techniques [6-9].

The development of the SGS combustion models is to occur in two stages. Only the first stage is discussed in this report. The first stage is to implement a simple, level I, combustion model into the CTH shock physics code to predict the first order effects of global heat release and product production. The model is based a Locally-Homogenous Flow (LHF) approximation for which state-relationships are identified between the reactive two-phase scalars and a passive scalar, the mixture fraction, that is tracked in the simulation [2-4]. The model assumes that the transport coefficients for each phase are equal, and molecular rates are sufficiently fast, so that local thermodynamic equilibrium is maintained. These approximations are appropriate for very small liquid or solid particles (*i.e.*, $D_p < 10\mu m$) undergoing rapid evaporation and have been applied successfully to the prediction of hydrocarbon fuel spray flames [3,5]. As a first step, the equation of state for each of these species is also assumed to follow a calorically perfect gas. However, multiphase flow effects can be included into the LHF approach and may be pursued in future efforts. The level I combustion model accounts for the effects of SGS turbulence through the use of a presumed mixture fraction FDF distribution, parameterized by its two lowest order moments, the mean and variance. This approach has been extensively used for prediction of gaseous hydrocarbon flames using LES [16-18], as well as for spray flames, using Reynolds Averaged Navier Stokes (RANS) formulations [3-5].

The second stage, level II, SGS combustion model is based on solving an evolution equation for composition and temperature JFDF using Monte Carlo methods. This approach has extensively been employed for the prediction of hydrocarbon diffusion flames with RANS [10,11] and only recently extended for application to LES [6-8]. The main advantage of the FDF approach is that, in theory, an arbitrarily detailed set of chemical kinetics may be employed. There are still many practical computational issues that are being addressed using this approach [12,13] and extension to muliphase systems is still an active area of research [19-24]. The level II modeling approach will not be addressed in this report but is briefly discussed as part of the future work in Chapter 4.

In the next Chapter, a description of the level I SGS combustion model, and its implementation into the Sandia's shock physics code, CTH, is provided. Results are presented in Chapter 3 for two classes of benchmark problems to assess the utility of the FDF approach. Lastly, in Chapter 4, conclusions are drawn from the findings of this study and future work suggested for improvements to the current model.

2. Mathematical Formulation and Implementation

The following describes the mathematical formulation and numerical implementation of the level I combustion model. It should be emphasized that the use of this model, in its current form, is restricted to gas phase, non-premixed, combustion systems. Specifically, the following should be considered when using the level I combustion model for any new application.

- **The level I combustion model is applicable for non-premixed systems only. The model does not account for any partial pre-mixing from local extinction or reignition events, nor any problem for which an oxidizer is dispersed along with the fuel. The only oxidizer that should be considered in the problem is the surrounding air. The level I combustion model will not capture the propagation of either a deflagration nor a detonation wave.**
- **The rate of combustion at the molecular level is assumed to be infinitely fast. It is assumed that as soon as the fuel and oxidizer come into contact, then they immediately react and form product.**
- **The combustion model is implemented using a calorically perfect gas equation of state. Extensions to multiphase, non-premixed, systems is possible within the context of the LHF assumption, but is outside the scope of the current work.**

2.1 Level I Combustion Model: A Presumed FDF Approach

In this study, a LES methodology is pursued where only the large scales of turbulent motion are resolved and a subgrid scale (SGS) model is employed to capture the integral effects of combustion processes. The SGS modeling approach is based on a probabilistic description of combustion using a locally homogeneous flow (LHF) approximation. In this approach, it is assumed there exists a unique state relationship between the reactive scalar composition and a passive scalar, the mixture fraction, Z [2]. The mixture fraction is defined locally as the amount of mass originating from the "fuel". The LHF approximation is appropriate for combustion problems that are mixing controlled such as hydrocarbon diffusion flames [2,25-28] or the burning of very fine clouds of solid or liquid fuel particulate (*i.e.,* Stokes number << 1) [3,5]. The functional form of the state relationship depends on, in general, the number of phases of the system and the chemical kinetic mechanisms. As an example, consider a simple, one-step, infinitely fast, $F + rOx \rightarrow (1 + r)P$ gas-phase reaction step, where F is the fuel, Ox is the oxidizer, P the product and r is the mass of oxidizer consumed per unit mass of fuel. It can be shown, that for this case, Y_i is a simple piece-wise linear function of Z [27,29], as illustrated below in Figure 2.1.

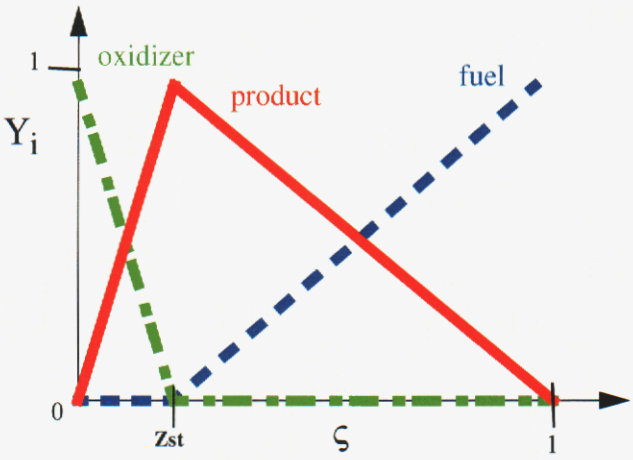

Figure 2.1: State-relationship for an infinitely fast one-step $F + rOx \rightarrow (1+r)P$ chemical kinetics for a gaseous system.

The reaction rate for each species is readily obtained by substituting the state-relationship (*i.e.*, $Y_i = Y_i(\varsigma)$) into the transport equation for that specie resulting in the following relation [25]:

$$\dot{\omega}_i''' = -\frac{1}{2}\rho\chi\frac{d^2Y_i}{d\varsigma^2}. \tag{2-1}$$

where χ $(= 2D_m\nabla Z \bullet \nabla Z)$ is the scalar dissipation rate and, physically, is a measure of the local loading rate of fuel and oxidizer into the flame zone. The reaction rate in Eq. (2-1) represents the production or destruction of a species through a laminar flame. The flamelet modeling approach for SGS combustion assumes the LES subgrid volume can be approximated as a superposition of burning laminar flames, or flamelets, as shown below in Figure 2.2.

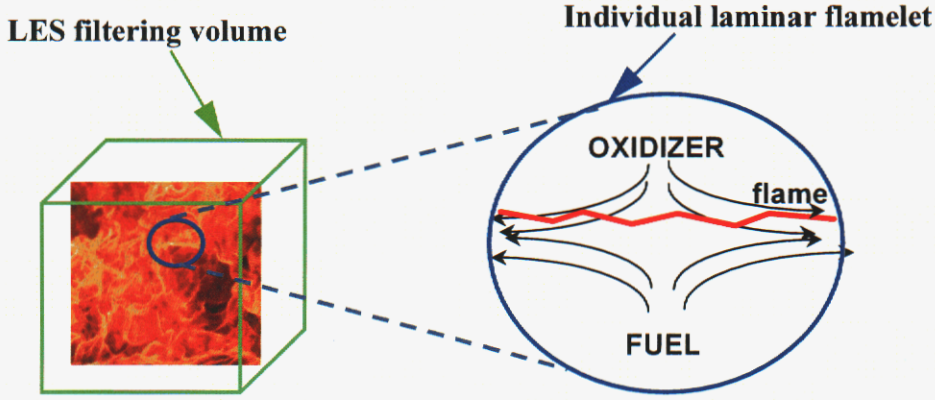

Figure 2.2: Ensemble of laminar flamelets representing subgrid scale combustion processes in LES filtering volume.

Summing over each flamelet, multiplied by its corresponding probability, results in the average or filtered reaction rate for the SGS volume. Since each flamelet is uniquely characterized by Z and χ, then the filtered reaction rate is determined by convoluting Eq. (2-1) with the JFDF of mixture fraction and its dissipation rate, $P_{z\chi}$ [30,31]:

$$\begin{aligned}\langle \dot{\omega}_i''' \rangle &= -\frac{1}{2}\int_0^{\chi_{max}}\int_0^1 P_{Z\chi}\rho(\varsigma)\chi\frac{d^2Y_i(\varsigma)}{d\varsigma^2}d\varsigma d\chi \\ &= -\frac{1}{2}\int_0^1 \langle\chi|\varsigma\rangle P_Z(\varsigma)\rho(\varsigma)\frac{d^2Y_i(\varsigma)}{d\varsigma^2}d\varsigma\end{aligned} \tag{2-2}$$

where $\langle\chi|\varsigma\rangle$ is defined as the conditionally averaged scalar dissipation rate. For highly turbulent flows, it may be assumed that the mixture fraction and its dissipation rate are statistically independent from each other [31], allowing for the JFDF to be expressed as the products of the FDFs of mixture fraction and scalar dissipation rate, *i.e.*, $P_{Z\chi} = P_Z P_\chi$, implying that $\langle\chi|\varsigma\rangle = \langle\chi\rangle$. The filtered chemical production rate thus becomes:

$$\langle \dot{\omega}_i''' \rangle = -\frac{1}{2}\langle\chi\rangle\int_0^1 P_Z(\varsigma)\rho(\varsigma)\frac{d^2Y_i(\varsigma)}{d\varsigma^2}d\varsigma. \tag{2-3}$$

It is worth noting that although the assumption of statistical independence of Z and χ may be appropriate for the problem of the dispersal of energetic material, more sophisticated approaches are required for transitionally turbulent reacting flows, such as pool fires [32]. Assuming infinitely fast reaction rates, then the second derivative of Y_i with respects to ς approaches a delta function at the stoichiometric value of mixture fraction, Z_{st}, allowing for an analytical solution to the convolution integral of Eq. (2-3).

$$\langle \dot{\omega}_i''' \rangle = -\frac{1}{2}C\langle\rho\rangle\langle\chi\rangle P_Z(Z_{st}) \tag{2-4}$$

In Eq (2-4), Z_{st} is the value of mixture fraction for which stoichiometric proportions of fuel and oxidizer exist, and is in general, a function of the chemical kinetics mechanism. For the simple one step, $F + rOx \rightarrow (1+r)P$ reaction, Z_{st} is defined as: $Z_{st} = 1/(1+r)$. The constant C in Eq. (2-4) is a function of the stoichiometric coefficients (to be defined) and $\langle\chi\rangle$ is the filtered dissipation rate and requires a model. Several approaches are available for modeling $\langle\chi\rangle$ including, simply neglecting the SGS effects (*i.e.*, $\langle\chi\rangle \approx 2D_m\nabla\langle Z\rangle \bullet \nabla\langle Z\rangle$) [15], employing models based

on either scale similarity principles[16], or assuming local turbulence equilibrium [34]. A review of some of these approaches can be found in the recent work of deBruynKops and Riley [33] and Jimenez *et al.* [34]. In this study, we choose to use the model of Jimenez *et al.* [34] where $\langle\chi\rangle$ is expressed in terms of the gradient of the SGS mixture fraction variance.

$$\langle\chi\rangle = \frac{(D_m + D_T)}{C_I\Delta_f^2}\nabla\sigma_Z^2 \tag{2-5}$$

In Eq (2-5), D_T is defined as the turbulent diffusivity and is modeled in terms of a turbulent eddy viscosity, ν_T $(= C_s\Delta_f|\langle S\rangle|)$, and a turbulent Schmidt number, Sc_T, using the relation: $D_T = \nu_T/Sc_T$. The SGS variance, σ_Z^2, is determined through a modeled evolution equation (to be discussed).

In addition to the filtered reaction rate, the filtered mass fractions are also required and determined by integrating the state relationship over P_Z:

$$\langle Y_i\rangle = \int_0^1 P_Z(\varsigma)Y_i(\varsigma)d\varsigma \tag{2-6}$$

Up to this point in the model development, the exact form of P_Z has not been specified. A beta function is assumed to adequately represent P_Z and has the following functional form:

$$P_Z(\varsigma) = \frac{\varsigma^{(\beta_1-1)}(1-\varsigma)^{(\beta_2-1)}}{\int_0^1 \varsigma'^{(\beta_1-1)}(1-\varsigma')^{(\beta_2-1)}d\varsigma'} = \frac{\Gamma(\beta_1+\beta_2)}{\Gamma(\beta_1)\Gamma(\beta_2)}(\varsigma^{(\beta_1-1)}(1-\varsigma)^{(\beta_2-1)}) \tag{2-7}$$

where Γ is defined as the gamma function [35]. The parameters β_1 ($\equiv\langle Z\rangle[\langle Z\rangle(1-\langle Z\rangle)/\sigma_Z^2 - 1]$) and β_2 ($\equiv(1-\langle Z\rangle)[\langle Z\rangle(1-\langle Z\rangle)/\sigma_Z^2 - 1]$) determine the shape of the FDF and are functions of the filtered mixture fraction, $\langle Z\rangle$, its variance, σ_Z^2. Eq. (2-7) is plotted in Fig. 2.3 for several values of subgrid variance and for (a) $\langle Z\rangle = 0.1$ and (b) $\langle Z\rangle = 0.5$. As shown, the beta function is able to reproduce a wide spectrum of mixing states ranging from an initially non-premixed state (*i.e.*, a double delta function) to a purely mixed state (*i.e.*, single delta function).

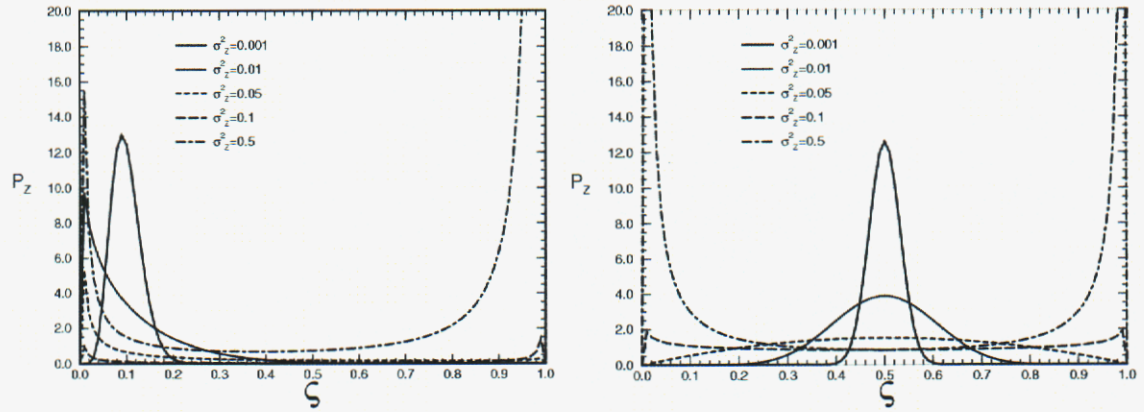

Figure 2.3: Beta FDF for several values of the subgrid variance and for filtered mixture equal to (a) 0.1 and (b) 0.5.

Substituting Eq. (2-7) into Eqs. (2-4) and (2-6), and assuming Y_i is a piece-wise linear function of Z, results in the following closed form analytical expressions for the filtered mass fraction and reaction rate for the ith species.

$$\langle Y_i \rangle = a_2 + (a_1 - a_2) I_{z_{st}}(\beta_1, \beta_2)$$

$$+ (b_1 - b_2)\frac{\beta_1}{\beta_1 + \beta_2}\left[I_{z_{st}}(\beta_1, \beta_2) + \frac{b_2}{b_1 - b_2} - \frac{\Gamma(\beta_1 + \beta_2)}{\Gamma(\beta_1)\Gamma(\beta_2)} \frac{Z_{st}^{\beta_1}(1 - Z_{st})^{\beta_2}}{\beta_1} \right] \tag{2-8}$$

$$\langle \dot{\omega}_i''' \rangle = -\frac{\langle \rho \rangle \langle \chi \rangle}{2} \frac{\Gamma(\beta_1 + \beta_2)}{\Gamma(\beta_1)\Gamma(\beta_2)} (b_2 - b_1) Z_{st}^{(\beta_1 - 1)} (1 - Z_{st})^{(\beta_2 - 1)} \tag{2-9}$$

In Eqs. (2-8) and (2-9), $I_{Z_{st}}$ is defined as the incomplete beta function [35]. The constants a an b are obtained from the infinitely fast state relationship, *i.e.*, $Y_i(z) = a + bZ$, where subscripts 1 and 2 denote the set of constants that are applicable for the lean (*i.e.*, $\varsigma < Z_{st}$) and rich (*i.e.*, $\varsigma > Z_{st}$) sides of Z_{st}, respectively. As an example, Figs. 2.4 (a) and (b) show the filtered mass fraction and reaction rate of CO_2 using methane-air chemical kinetics for several values of σ_Z^2. As shown, increasing the value of σ_Z^2 results in lower values of filtered mass fraction and reaction rate due to an increase in subgrid turbulent mixing.

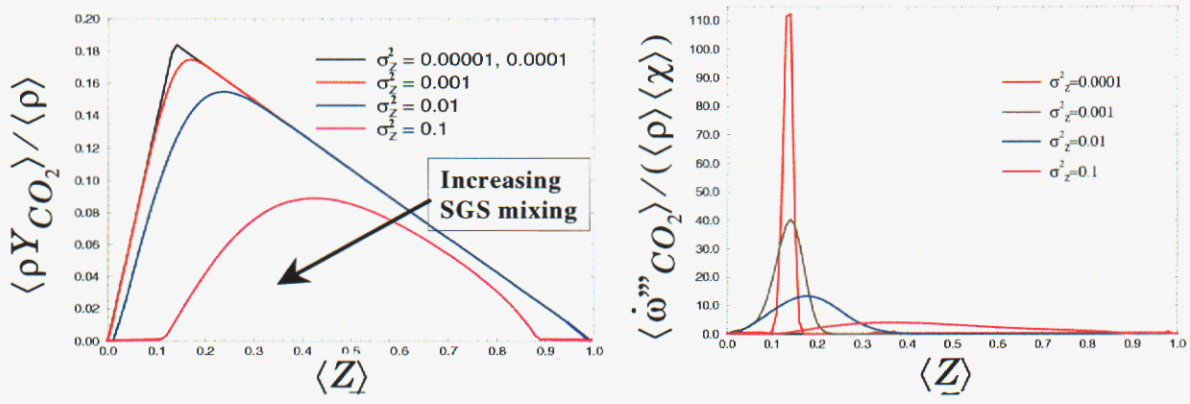

(a) (b)

Figure 2.4: Filtered CO_2 (a) mass fractions and (b) reaction rates for several values of subgrid variance assuming infinitely fast chemical kinetics.

In Eqs. (2-8) and (2-9), $\langle Z \rangle$ and σ_Z^2 are required for evaluating the filtered mass fractions and reaction rates. A gradient diffusion turbulence model is used for the $\langle Z \rangle$ transport equation:

$$\langle \rho \rangle \frac{D\langle Z \rangle}{Dt} = \nabla \bullet [(D_m + D_T) \nabla \langle Z \rangle] \tag{2-10}$$

where D_m and D_T are the molecular and turbulent diffusivity, respectively. Analogous to the approaches available for modeling $\langle \chi \rangle$, closure for σ_Z^2 include scale-similarity[16] and one-equation modeling approaches [34]. In this study we choose the one-equation model of Jimenez *et al.* [34],

$$\langle \rho \rangle \frac{D\sigma_Z^2}{Dt} = \underbrace{\nabla \bullet [\langle \rho \rangle (D_m + D_T) \nabla \sigma_Z^2]}_{Dif} + \underbrace{2\langle \rho \rangle (D_m + D_T) \nabla \langle Z \rangle \bullet \nabla \langle Z \rangle}_{\wp} - \underbrace{\langle \rho \rangle 2 \langle D_m \nabla Z \bullet \nabla Z \rangle}_{\langle \chi \rangle} \tag{2-11}$$

where the Dif, $\wp$ and $\langle \chi \rangle$ terms represent the diffusion, production and dissipation rates of σ_Z^2. In Eq. (2-11), Dif and $\wp$ are in closed form and known, while $\langle \chi \rangle$ requires a model and is closed using Eq. (2-5).

2.2 Chemical Kinetics Schemes

Three one-step, infinitely fast, chemical kinetics mechanisms are considered in this study. The

first kinetics scheme considered is a general hydrocarbon fuel, C_mH_n, burning with air having the following one-step reaction mechanism.

$$C_mH_n + \left(m + \frac{n}{4}\right)(O_2 + 3.76N_2) \rightarrow mCO_n + \frac{n}{2}H_2O + 3.76\left(m + \frac{n}{4}\right)N_2 \qquad (2\text{-}12)$$

The state-relationships for this mechanism are shown below in Fig. 2.5,

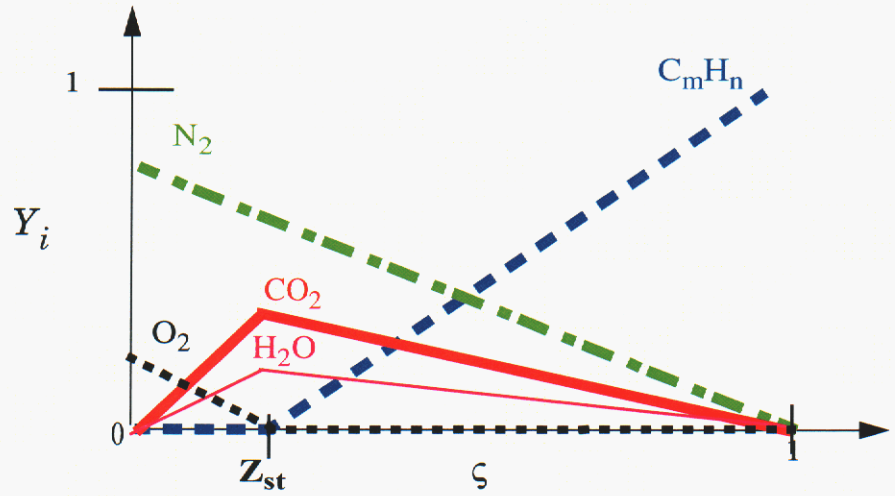

Figure 2.5: State-relationships for infinitely fast, gaseous, hydrocarbon-air combustion.

and may be represented using the following functions that are broken into two piece-wise linear regions before (lean side) and after (rich side) the stoichiometric value of mixture fraction, Z_{st}:

for $\varsigma < Z_{st}$

$$Y_{C_mH_n} = 0$$

$$Y_{N_2} = (1-\varsigma)\frac{3.76MW_{N_2}}{3.76MW_{N_2} + MW_{O_2}}$$

$$Y_{O_2} = (1-\varsigma/Z_{st})\frac{MW_{O_2}}{3.76MW_{N_2} + MW_{O_2}}$$

$$Y_{CO_2} = \left(\frac{\varsigma}{Z_{st}}\right)\frac{mMW_{CO_2}}{Den}$$

$$Y_{H_2O} = \left(\frac{\varsigma}{Z_{st}}\right)\frac{(nMW_{H_2O})/2}{Den}$$

for $\varsigma \geq Z_{st}$

$$Y_{C_mH_n} = (\varsigma - Z_{st})/(1-Z_{st})$$

$$Y_{N_2} = (1-\varsigma)\frac{3.76MW_{N_2}}{3.76MW_{N_2} + MW_{O_2}}$$

$$Y_{O_2} = 0$$

$$Y_{CO_2} = \left(\frac{1-\varsigma}{1-Z_{st}}\right)\frac{mMW_{CO_2}}{Den}$$

$$Y_{H_2O} = \left(\frac{1-\varsigma}{1-Z_{st}}\right)\frac{(nMW_{H_2O})/2}{Den}$$

where $Z_{st} = (mMW_C + nMW_H)/Den$ and $Den = mMW_{CO_2} + (nMW_{H_2O})/2 + 3.76MW_{N_2}(m + n/4)$.

The second fuel type considered is a general fluorocarbon fuel, C_mF_n, burning with air having the following one-step reaction mechanism.

$$C_mF_n + m(O_2 + 3.76N_2) \rightarrow mCO_2 + \frac{n}{2}F_2 + 3.76mN_2 \qquad (2\text{-}13)$$

The state-relationships for this cases are shown below in Fig. 2.6,

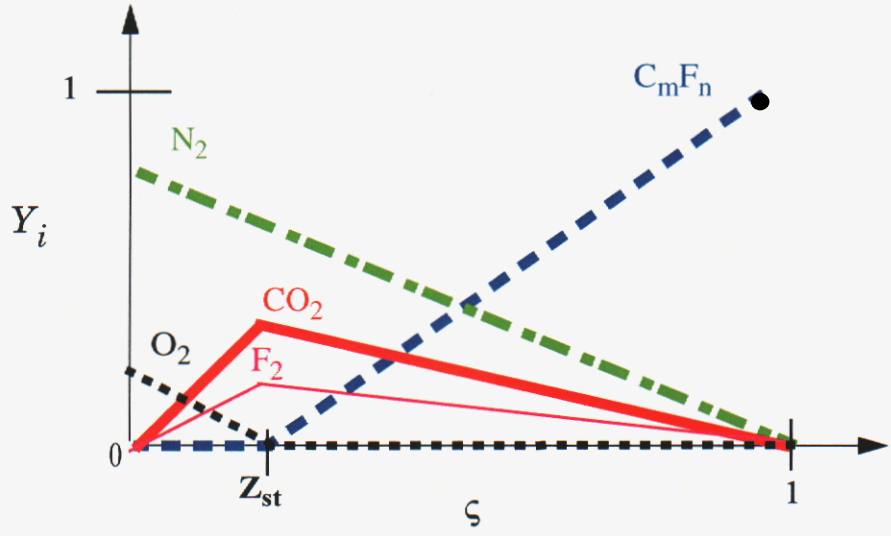

Figure 2.6: State-relationships for infinitely fast, gaseous, fluorocarbon-air combustion.

and may be expressed using the following relations:

for $\varsigma < Z_{st}$

$$Y_{C_mF_n} = 0$$

$$Y_{N_2} = (1-\varsigma)\frac{3.76MW_{N_2}}{3.76MW_{N_2} + MW_{O_2}}$$

$$Y_{O_2} = (1-\varsigma/Z_{st})\frac{MW_{O_2}}{3.76MW_{N_2} + MW_{O_2}}$$

$$Y_{CO_2} = \left(\frac{\varsigma}{Z_{st}}\right)\frac{mMW_{CO_2}}{D}$$

$$Y_{F_2} = \left(\frac{\varsigma}{Z_{st}}\right)\frac{(nMW_{H_2O})/2}{D}$$

for $\varsigma \geq Z_{st}$

$$Y_{C_mF_n} = (\varsigma - Z_{st})/(1-Z_{st})$$

$$Y_{N_2} = (1-\varsigma)\frac{3.76MW_{N_2}}{3.76MW_{N_2} + MW_{O_2}}$$

$$Y_{O_2} = 0$$

$$Y_{CO_2} = \left(\frac{1-\varsigma}{1-Z_{st}}\right)\frac{mMW_{CO_2}}{D}$$

$$Y_{F_2} = \left(\frac{1-\varsigma}{1-Z_{st}}\right)\frac{(nMW_{H_2O})/2}{D}$$

where $Z_{st} = (mMW_C + nMW_F)/Den$ and $Den = mMW_{CO_2} + (nMW_{F_2})/2 + 3.76mMW_{N_2}$.

The third fuel type is a metal fuel, M, burning with air having the following one-step kinetics scheme.

$$M + \frac{n}{2}(O_2 + 3.76N_2) \rightarrow MO_n + 3.76\frac{n}{2}N_2 \qquad (2\text{-}14)$$

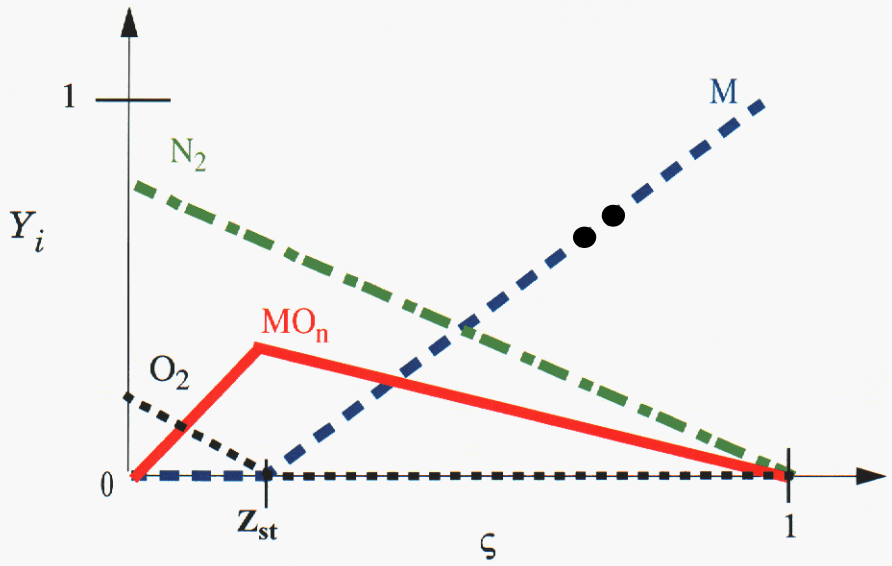

Figure 2.7: State-relationships for infinitely fast, gaseous, metal-air combustion.

The state-relationships for this fuel are given as:

$$\underline{\text{for } \varsigma < Z_{st}}$$

$$Y_M = 0$$

$$Y_{N_2} = (1-\varsigma)\frac{3.76MW_{N_2}}{3.76MW_{N_2} + MW_{O_2}}$$

$$Y_{O_2} = (1-\varsigma/Z_{st})\frac{MW_{O_2}}{3.76MW_{N_2} + MW_{O_2}}$$

$$Y_{MO_n} = \left(\frac{\varsigma}{Z_{st}}\right)\frac{MW_{MO_n}}{Den}$$

$$\underline{\text{for } \varsigma \geq Z_{st}}$$

$$Y_M = (\varsigma - Z_{st})/(1 - Z_{st})$$

$$Y_{N_2} = (1-\varsigma)\frac{3.76MW_{N_2}}{3.76MW_{N_2} + MW_{O_2}}$$

$$Y_{O_2} = 0$$

$$Y_{MO_n} = \left(\frac{1-\varsigma}{1-Z_{st}}\right)\frac{MW_{MO_n}}{Den}$$

where $Z_{st} = MW_M/Den$ and $Den = n(3.76MW_{N_2} + MW_{O_2})/2 + MW_M$.

2.3 Numerical Implementation into CTH

Three main numerical considerations are addressed with regard to the implementation of the level I combustion model into CTH. They are, in order of importance, i) support of multi-component species in the equation of state, ii) discretization of transport equations for the filtered mixture fraction and its variance and iii) use of the pressure gradient scaling techniques for efficient temporal integration at low Mach number flows. The following discusses each of these issues in further detail.

2.3.1 Support of Multiple Species Equation of State

As a starting point, the LMMSC EOS in CTH is adapted for use with the level I combustion model. In this EOS, the thermodynamic properties of each specie are determined using the following set of relations,

$$\begin{aligned} C_{v_i} &= \Re(1.5 + 0.5\xi)/MW_i \\ \gamma_i &= C_{P_i}/C_{v_i} = (2.5 + 0.5\xi)/(1.5 + 0.5\xi) \end{aligned} \tag{2-15}$$

where ξ is number of rotational degrees of freedom and set equal to 2 for a linear molecule and 3 for a nonlinear molecule. The LMMSC routines are modified by first determining the composition of the material using (2-8), then the mixture weighted properties are determined using standard mass weighting rules for ideal gases [30].

2.3.2 Discretization of Transport Equations

The transport equations of Eqs. (2-10) and (2-11) are added to CTH in the Lagrangian and remap steps that currently reside in the code. In the Lagrangian step, the left-hand-side (substantial derivative) and the first term on the right-hand-side (diffusion term) of Eqs. (2-10) and (2-11) are advanced in time. The effects of the turbulent diffusion term being introduced as part of the flux limiting scheme [36,37] and may be thought of a MILES approach to treating the advection and subgrid turbulent mixing processes [38]. The production and dissipation terms in Eq. (2-11) are incorporated as part of the remap advancement where Eq. (2-11) may be descretized using the following semi-implicit form (assuming $D_T \gg D_m$):

$$\frac{\sigma_Z^{2(t+\Delta t)} - \sigma_Z^{2(t)}}{\Delta t} = \wp^{(t)} + \langle \chi \rangle^{(t+\Delta t)} = \wp^{(t)} + [D_T^{(t)}/(C_I \Delta_f^2)] \nabla \sigma_Z^{2(t+\Delta t)} \tag{2-16}$$

where the turbulent dissipation term is treated implicitly to maintain stability. Eq. (2-16) may be re-arranged for explicit evaluation of $\sigma_Z^{2(t+\Delta t)}$.

$$\sigma_Z^{2(t+\Delta t)} = [\sigma_Z^{2(t)} + \Delta t \, \wp^{(t)}]/(1 + \Delta t D_T^{(t)}/C_I \Delta_f^2) \tag{2-17}$$

In addition to updating Eqs. (2-10) and (2-11), a chemical source term is also added to the energy equation using the source term of Eq. (2-9). A simple Eulerian time advancement is used for this purposes and found to be stable for all the cases considered,

$$E^{(t+\Delta t)} = E^{(t)} - \Delta t \sum_{i=1}^{N} \langle \dot{\omega}_i''' \rangle h_{f_i}^o \tag{2-18}$$

where $h_{f_i}^{o}$ is the heat of formation of the i^{th} species.

2.3.3 Numerical Integration for Low Speed Flows

Simulation of a secondary combustion event requires numerical integration over very long periods of time, relative to a shock event, in order to capture the long term effects of turbulent mixing. Several algorithms exist for efficient time integration for low-speed flows. However, many of these approaches require the solution of a pressure Poisson equation that would require a significant level of effort to implement into the existing CTH framework. Rather than pursuing this approach, the pressure gradient scaling (PGS) technique of Ramshaw *et al.* [39,40] is adapted. In PGS, the hyperbolic system of equations is modified in such a way that the eigenvalues associated with entropy and contact surfaces are unaffected while the propagation speeds of the acoustic waves are artificially reduced. For flows with small pressure gradients these waves may be altered so that they still propagate fast relative to the advection processes in the problem, but still much slower than the original acoustic waves. This approach may be compared to more modern pseudo-compressibility methods or preconditioning schemes [41-46] that have originated from the pioneering work of Chorin [47]. The main difference between the PGS approach and these other methods is that often pseduo-time subcyling is employed for the latter while the PGS approach does not impose these requirements. The rest of the details on the implementation of PGS into CTH and the necessary changes to the non-reflective boundary condition may be found in appendix A.

3. Results

3.1 Individual Fuel Fragment Combustion

The first benchmark problem considered using the level I combustion model is the burning of an isolated ball of fuel. This problem may be thought of as an idealization of an isolated piece of burning material which is thrown from an explosion event. The initial conditions for this problem are shown below in Fig. 3.1.

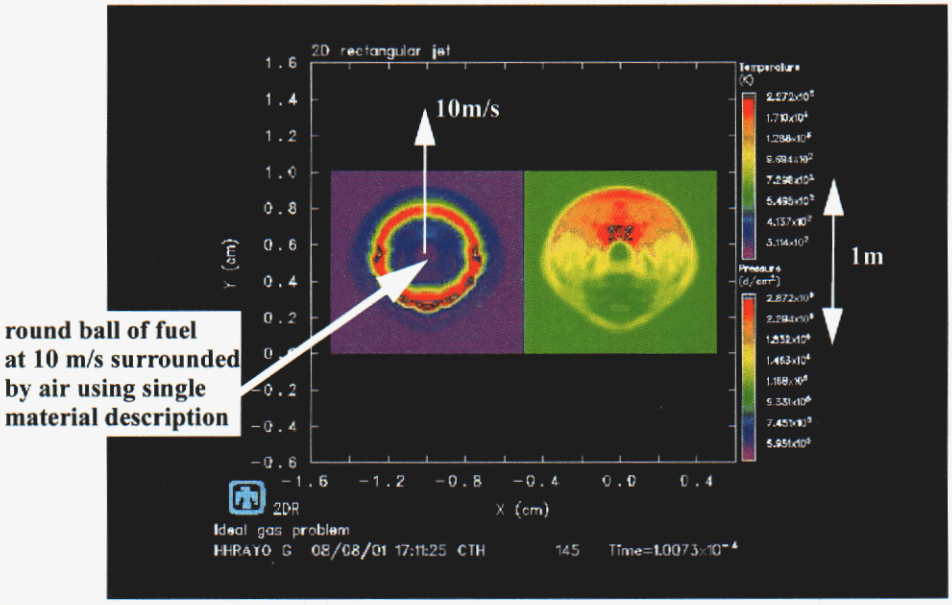

Figure 3.1: Initial conditions for reacting fuel fragment problem.

Methane is chosen as the fuel and initialized with a 10 m/s upward velocity. Figs 3.2 (a) and (b) show instantaneous snapshots of temperature and pressure contours during the simulation after 0.5 and 1.7 ms, respectively. As expected, a flame is established at the fuel-air interface and is subsequently stretched and distorted as the fuel is mixed in with the surrounding air. After approximately 10 ms, the fuel is completely consumed and the temperature of the domain reaches the adiabatic flame temperature.

This problem also serves as a test case to examine the speed-up gained by incorporating the PGS technique into CTH. Figure 3.3 shows the time evolution of the ratio of the modified time step using PGS, divided by the original time step, as a function of time. A speedup of approximately 30 is observed early in the simulation up to 0.1 ms in time and eventually reaches a nominal steady-state value of 15 after 0.2 ms. The speed-up for this case may be considered optimistic since the pressure gradients are small throughout the simulation. Problems involving the propagation of a shock wave can be expected to experience overall speedup gains for an entire simulation, but less than the gains observed for this case.

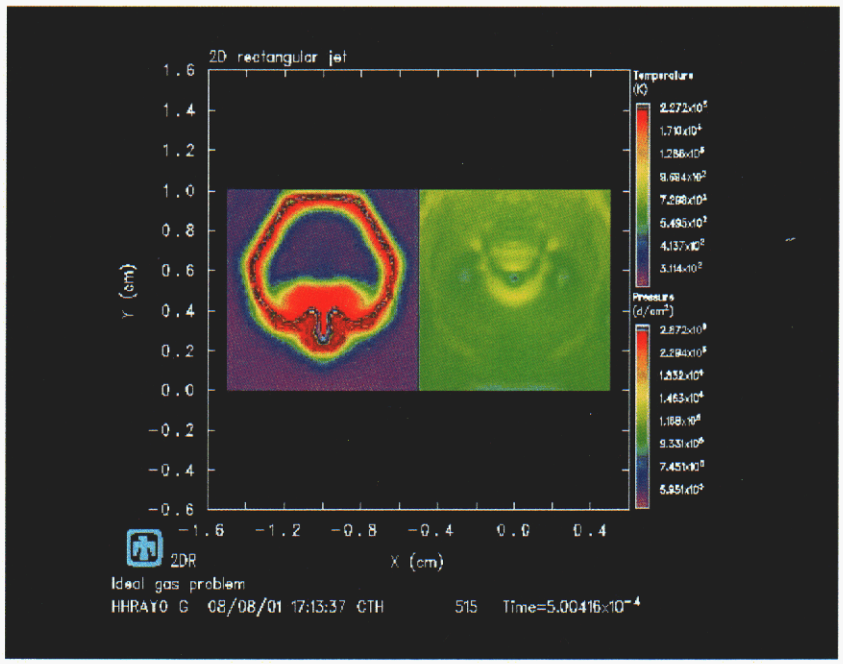

(a)

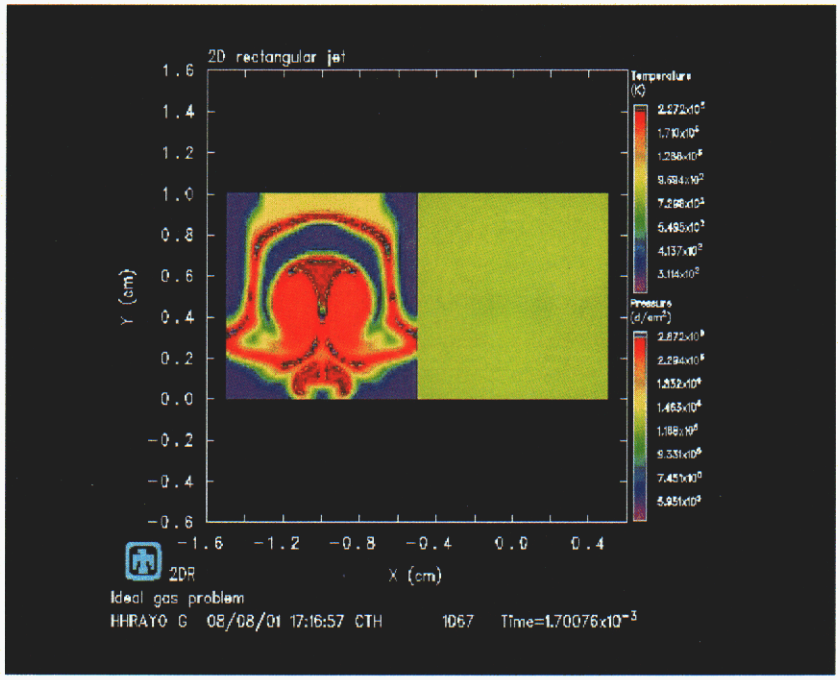

(b)

Figure 3.2: Instantaneous snapshots of temperature and pressure contours at (a) 0.5 ms and (b) 1.7 ms

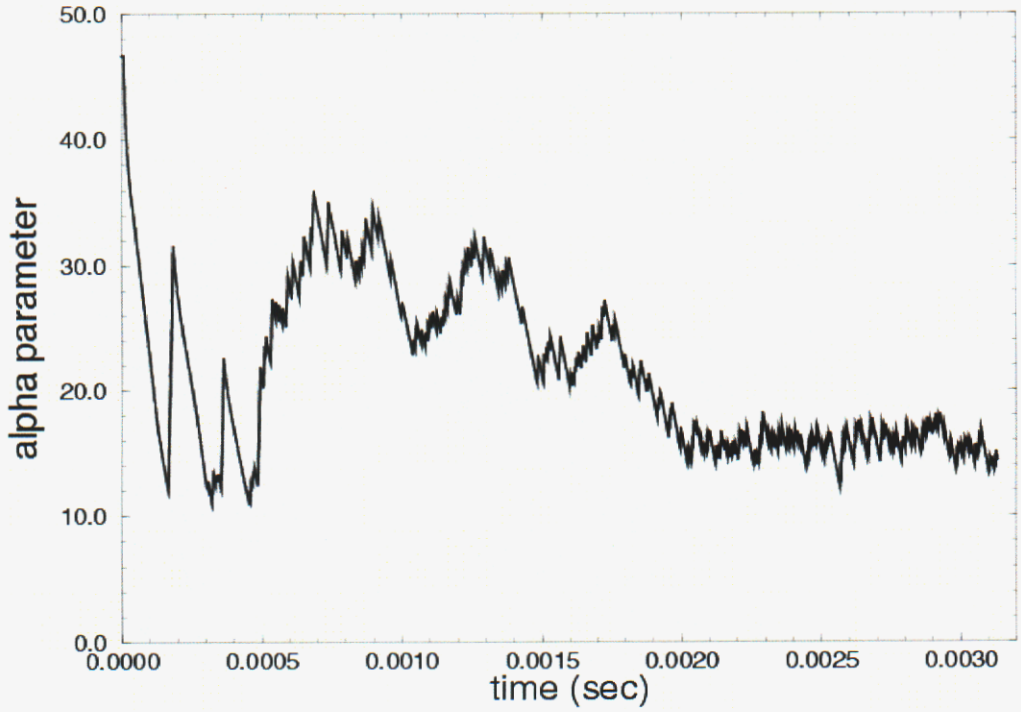

Figure 3.3: Speedup of CTH time stepping algorithm using PGS as a function of time.

3.2 Shock Induced Dispersal and Combustion of Energetic Material

The second benchmark problem considered is the dispersal of a fuel from detonation of a high explosive. The initial conditions for this problem are shown in Fig. 3.4 and consist of a high-explosive charge surrounded by a thin aluminum shell that is filled with a gaseous combustible magnesium material. A detonation wave is propagated through the propellant and is prescribed using the HEBURN option in CTH. After the detonation event ($\sim 30\ \mu s$), the high temperature and pressure in the chamber causes rupture of the aluminum shell and dispersal of the magnesium gas into the surrounding air. Two simulations were performed. The first case is without the combustion model activated and the second case is with the model activated.

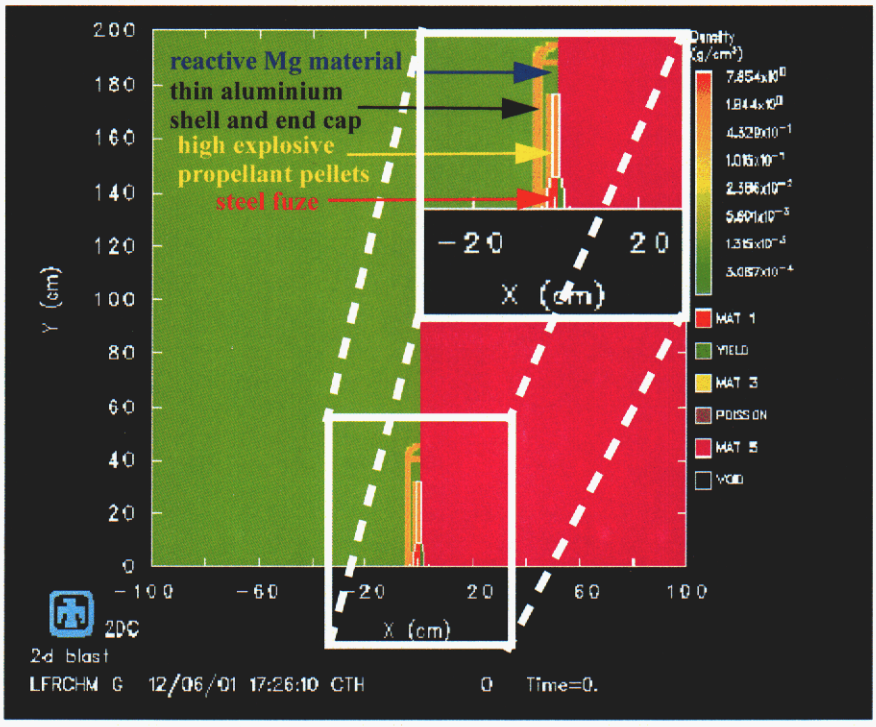

Figure 3.4: Computational domain and initial conditions for modeled shock induced dispersal problem. Inset shows near field region of energetic material package.

Figures 3.5 and 3.6 show snapshots of the temperature and pressure fields during the simulation at 0.5 and 3.3 ms, respectively, without (a) and with (b) the combustion model activated. Figs. 3.5 (a) and (b) show the combustion model has little effect on the temperature and pressure fields very early in the dispersal process due to the limited amount of turbulent mixing with the surrounding air. A larger difference can be seen in Figs. 3.6 (a) and (b) where the burning of the magnesium material results in higher temperatures at the interfaces between the ejected material and surrounding air.

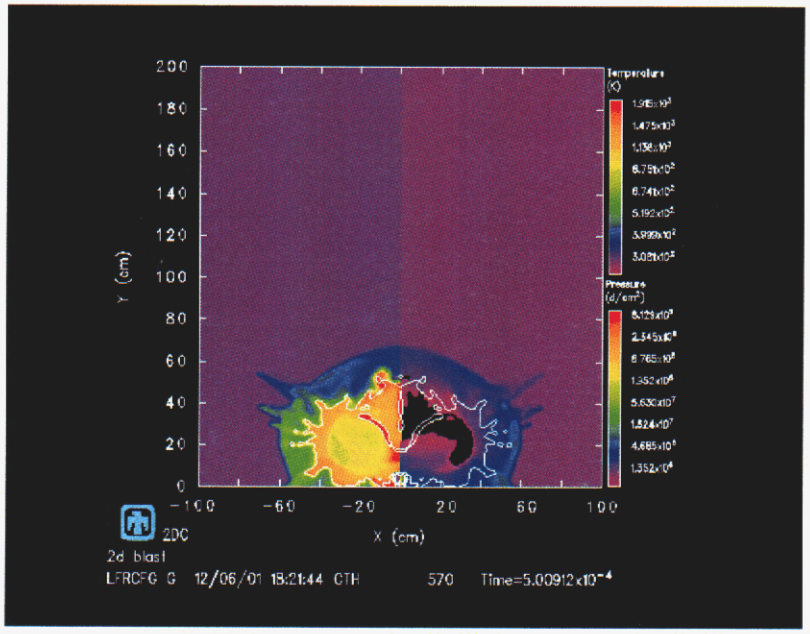

(a)

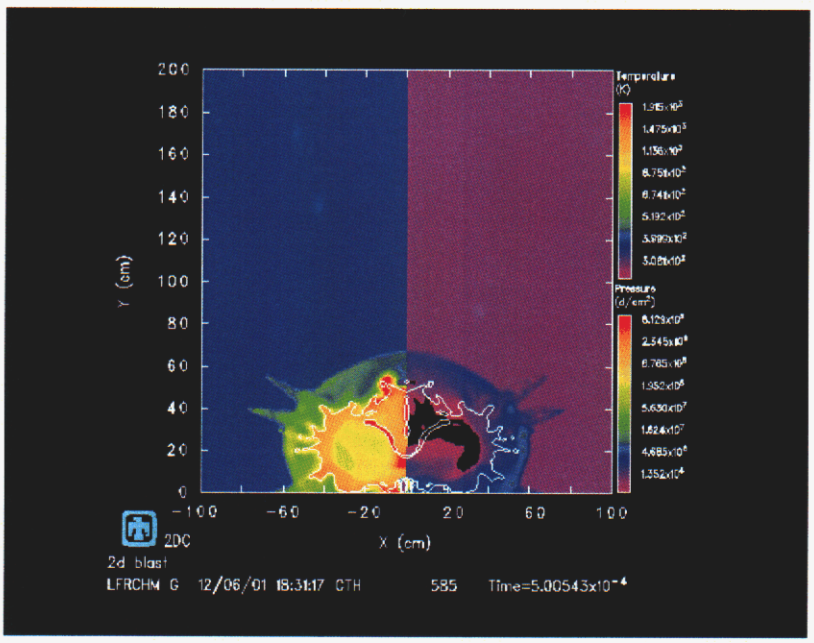

(b)

Figure 3.5: Instantaneous snapshot of temperature and pressure contours after 0.5 ms (a) without and (b) with SGS combustion model activated.

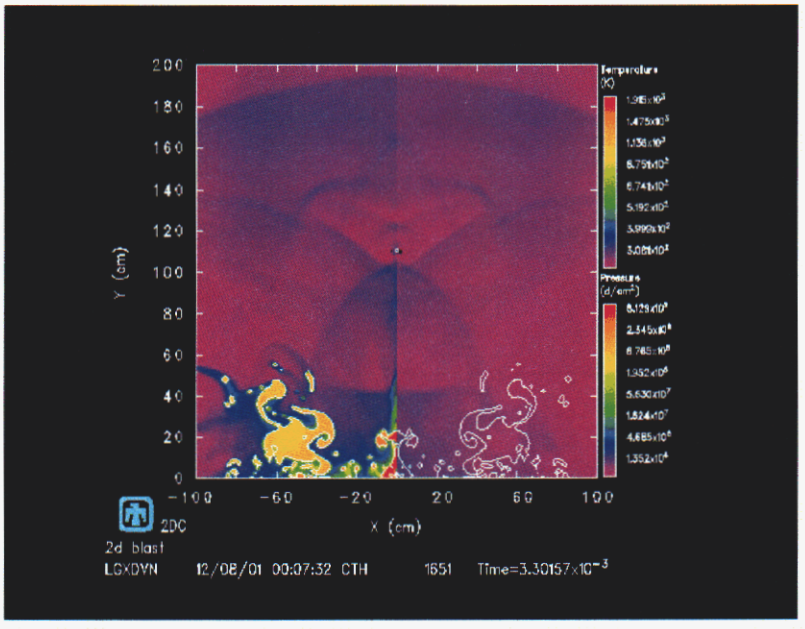

(a)

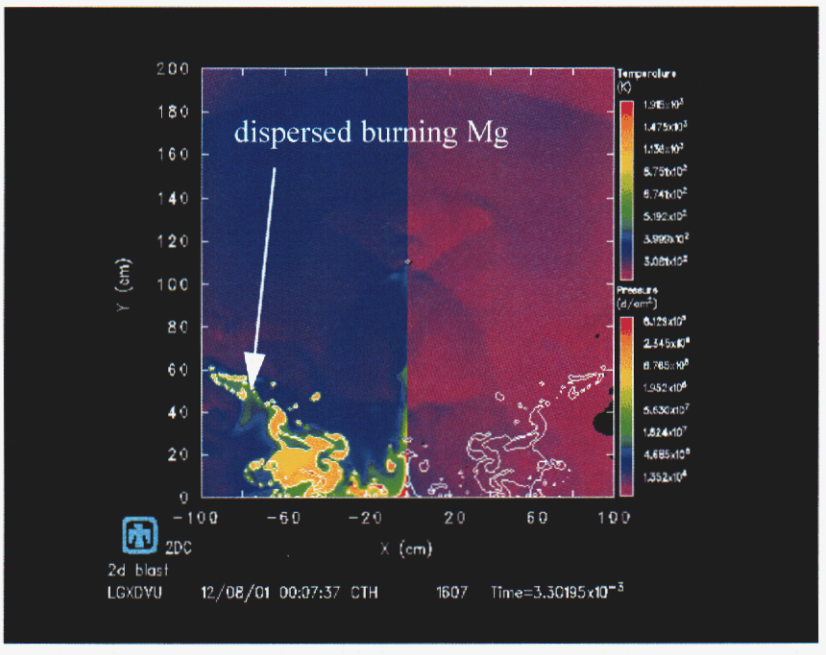

(b)

Figure 3.6: Instantaneous snapshot of temperature and pressure contours after 3.3 ms (a) without and (b) with SGS combustion model activated.

4. Summary and Conclusions

4.1 Accomplishments

In this exploratory, one-year study, a level I combustion model is developed and successfully implemented into the CTH shock physics code. Two classes of benchmark problems are examined for use with the model. The first is the burning of an individual fuel fragment and the second is the shock-induced dispersal and combustion of an energetic material. In addition to the combustion model development, the CTH time stepping algorithm is improved to allow for efficient integration at relatively low speed flows. Specifically, the following tasks were completed.

- Improvement of the CTH time-stepping algorithm using PGS techniques to allow for efficient integration at low speeds. Modification of the non-reflective boundary condition to maintain compatibility with use of PGS.
- Re-incorporation of multi-component species EOS into the current version of CTH.
- Development and implementation of level I combustion model into CTH. The model is based on conserved scalar, flamelet modeling methodology with three single-step chemistry mechanisms for use with gaseous hydrocarbon, fluorocarbon and metal fuels.
- Time stepping changes and SGS combustion modeling exercised for several benchmark problems.

4.2 Recommendations for Future Research

The level I combustion developed in this study is limited to gas phase mixtures for which the combustion is largely mixing controlled. Within these approximations, a shock driven dispersal and combustion event can be analyzed to study the first order effects of heat release on overall turbulent mixing and flow development. For a predictive capability, the current methodology needs to be extended to multiphase formulations with complex chemistry. The level I combustion model can be extended to simple multiphase systems within the context of using a locally homogeneous flow (LHF) approximation [3,4]. This approach would consist of establishing state-relationships for both the liquid, solid and gas phases and would allow analysis of simple non-premixed, two-phase systems containing small particles of dispersed reactive material. However, for more complicated systems involving significant heat and mass transfer between phases, a more generalized approach must be pursued. One approach for achieving this ambitious goal is the use of probabilistic descriptions of multiphase flow systems using Monte Carlo techniques. These approaches have shown to be successful for RANS calculations [23,24] but have not been extended to LES formulations. The recommendation from this study is to pursue the development of FDF approaches to multiphase flows based on the RANS two-phase flow work of Refs. [23,24] and the reacting flow LES studies using FDF from Refs. [6-8]. The expected increase in predictive capability will, however, come at a steep computational cost that is estimated to be at least one order of magnitude greater than the current level I combustion model. The main challenge

will then be to develop practical solutions for performing large scale computations using Monte Carlo methods.

References

[1] Bell, R.L., Baer, M.R., Brannon, R.M., Cole, R.A., Crawford, D.A., Elrick, M.G., Hertel, E.S., Silling, S.A. and Taylor, P.A., "CTH User's manual and input instructions," JAN02 version of CTH, Sandia National Laboratories, 2002.

[2] Faeth, G.M., "Mixing, transport and combustion in sprays," *Combust. and Flame*, vol. 30, pp. 277-284, 1977.

[3] Faeth, G.M., "Evaporation and combustion in sprays," *Prog. Energy Combust. Sci.*, vol. 9, pp. 1-76, 1983.

[4] Faeth, G.M., "Mixing, transport and combustion in sprays," *Prog. Energy Combust. Sci.*, vol. 13, pp. 293-345, 1987.

[5] Iyer, V.A., Abraham, J. and Magi, V., "Exploring injected droplet size effects on steady liquid penetration in a Diesel spray with a two-phase model," *Int. J. of Heat and Mass Trans.*, vol. 45, pp. 519-531, 2002.

[6] Colucci, P. J., Jaberi, F. A., Givi, P. and Pope, S. B., "Filtered density function for large eddy simulation of turbulent reacting flows," *Phys. Fluids*, Vol. 10, pp. 499-515, 1998.

[7] Jaberi, F.A., Colucci, P.J., James, S., Givi, P., Pope, S.B., "Filtered mass density function for large-eddy simulation of turbulent reacting flows," *J. Fluid Mech.*, pp. 85-121, 1999.

[8] Zhou, X.Y. and Pereira, J.C.F., "Large Eddy Simulation (2D) of a reacting plane mixing layer using filtered density function closure," *Flow, Turbulence and Combustion*, vol. 64, pp. 279-300, 2000.

[9] Pope, S. B., "Computations of turbulent combustion: progress and challenges," In *Twenty-Third Symp. (Int.) on Combustion*, pp. 591-612, Pittsburgh: The Combustion Institute, 1990.

[10] Pope, S. B., "PDF methods for turbulent reactive flows," *Prog. Energy Combust. Sci.*, vol. 11, pp. 119-192, 1985.

[11] Xu, J. and Pope, S.B., "PDF calculations of turbulent nonpremixed flames with local extinction," *Combust. and Flame*, vol. 123, pp. 281-307, 2000.

[12] Pope, S. B., "Computationally efficient implementation of combustion chemistry using *in situ* adaptive tabulation," *Combustion Theory and Modeling*, vol. 1, no. 1, pp. 41- 63, 1997.

[13] Xu, J. and Pope, S.B., "Assessment of numerical accuracy of PDF/Monte Carlo methods for turbulent reacting flows," *J. of Comput. Phys.*, vol. 152, pp. 192-230, 1999.

[14] DesJardin, P.E. and Frankel, S.H., "Large eddy simulation of a nonpremixed reacting jet: Application and assessment of subgrid-scale combustion models," *Phys. Fluids*, vol. 10, pp. 2298-2314, 1998.

[15] Pierce, C.D. and Moin, P., "A dynamic model for subgrid variance and dissipation rate of a conserved scalar," *Phys. Fluids*, vol. 10, pp. 3041, 1998.

[16] DesJardin, P.E. and Frankel, S.H., "Large eddy simulation of soot formation in the near-Field of a strongly radiating nonpremixed acetylene-air turbulent jet flame," *Combust. and Flame*, vol. 119, pp. 121-132, 1999.

[17] Wall, C., Jan Boersma, B. and Moin, P., "An evaluation of the assumed beta probability density function subgrid-scale model for large eddy simulation of nonpremixed, turbulent combustion with heat release," *Phys. Fluids*, vol. 12, pp. 2522-2529, 2000.

[18] Pitsch, H. and Steiner, H., "Large-eddy simulation of a turbulent piloted methane/air diffusion flame (Sandia flame D)," *Phys. Fluids*, vol. 12, pp. 2541-2554, 2000.

[19] Williams, F.A., Combustion Theory, 2nd ed., Benjamin/Cummings, Menlo Park, 1985.

[20] Zhu, M., Bray, K.N.C. and Rogg, B., "PDF modeling of spray autoignition in high pressure turbulent flows," *Combust. Sci. and Tech.*, vol. 120, pp. 357-379, 1996.

[21] Dukowicz, J.K., "A particle-fluid numerical model for liquid sprays," *J. of Comput. Phys.*, vol. 35, pp. 229-253, 1980.

[22] Jones, W.P. and Sheen, D.-H., "A probability density function method for modelling liquid fuel sprays," *Flow, Turbulence and Combustion*, vol. 63, pp. 379-394, 1999.

[23] Rumberg, O. and Rogg, B., "Full PDF modelling of reactive sprays via an evaporation-progress variable," *Combust. Sci. and Tech.*, vol. 158, pp. 211-247, 2000.

[24] Zhu, M., Bray, K.N.C., Rumberg, O. and Rogg, B., "PDF transport equations for two-phase reactive flows and sprays," *Combust. and Flame*, vol. 122, pp. 327-338, 2000.

[25] Bilger, R. W., "Reaction rates in diffusion flames," *Combust. and Flame*, Vol. 30, 1977, pp. 277-284.

[26] Peters, N., "Laminar diffusion flamelet models in non-premixed turbulent combustion," *Energy Combust. Sci.*, Vol. 10, pp. 319-339, 1984.

[27] Peters, N., "Laminar flamelet concepts in turbulent combustion," *Twenty-first Symp. (Int.) on Combustion*, The Combustion Institute, Pittsburgh, PA, pp. 1231-1250, 1986.

[28] Peters, N., Turbulent Combustion, Cambridge University Press, Cambridge, U.K., 2000.

[29] William, F.A., "Progress in knowledge of flamelet structure and extinction," *Prog. in*

Energ. and Comb. Sci., vol. 26, pp. 657-682, 2000.

[30] Kuo, K. K., Principles of Combustion, Wiley, 1986, p. 460.

[31] Cook, A. W., Riley, J. J. and Kosaly, G., "A Laminar flamelet approach to subgrid-scale chemistry in turbulent flows," *Combust. and Flame*, Vol. 109, pp. 332-341, 1997.

[32] DesJardin, P.E., Smith, T.M. and Roy, C.J., "Numerical simulations of a methanol pool fire," AIAA Paper, AIAA-01-0636, 2001.

[33] deBruynKops, S.M. and Riley, J.J., "Mixing models for large-eddy simulation of non-premixed turbulent combustion," *ASME Journal of Fluids Engineering*, vol. 123, pp. 341-346, 2001.

[34] Jimenez, C., Ducros, F., Cuenot, B. and Bedat, B., "Subgrid scale variance and dissipation of a scalar field in large eddy simulations," *Phys. Fluids*, vol. 13, pp. 1748-1754, 2001.

[35] Advanced Engineering Mathematics, Fifth Edition, Wylie, C.R. and Barrett, L.C., McGraw-Hill Publishing Company, 1982.

[36] Van Leer, B., "Towards the ultimate conservation difference scheme. IV. A new approach to numerical convection," *J. of Comput. Phys.*, vol. 23, pp. 276-299, 1977.

[37] McGlaun, M. J., "Improvements in CSQII: an improved numerical convection algorithm", Sandia National Laboratories Report, SAND82-0051, 1982.

[38] Grinstein, F.F. and Fureby, C., "Recent progress on miles for high Reynolds-number flows," AIAA paper, AIAA 2002-0134, 2002.

[39] O'Rourke, P.J. and Bracco, F.V., "Two scaling transformations for the numerical computation of multidimensional unsteady laminar flames," *J. of Comput. Phys.*, vol. 33, pp. 185-203, 1979.

[40] Ramshaw, J. D., O'Rourke, P. J. and Stein, L. R., "Pressure gradient scaling method for fluid flow with nearly uniform pressure," *J. of Comput. Phys.*, Vol. 58, pp. 360-376, 1985.

[41] Kim, W-W, Menon, S., "An unsteady incompressible Navier-Stokes solver for large eddy simultion of turbulent flows," *Int. J. for Num. Methods in Fluids*, vol. 31, pp. 983-1017, 1999.

[42] Van Leer, B., Wen-Tzong, L. and Roe, P., "Characteristic time-stepping or local preconditioning of the Euler equations," AIAA paper, AIAA 91-40726, 1991.

[43] Godfrey, A.G., Walters, R.W. and Van Leer, B., "Preconditioning for the Navier-Stokes equations with finite-rate chemistry," AIAA paper, AIAA-93-0535, 1993.

[44] Merkle, C. L. and Choi, Y., "Computation of low-speed flow with heat addition," *AIAA J.*, vol. 25, no. 6, pp. 831-838, 1986.

[45] Chen, K.-H and Pletcher, R.H., "Primitive variable, strongly implicit calculation procedure for viscous flows at all speeds," *AIAA J.*, vol. 29, no. 8, pp. 1241-1249.

[46] Edwards, J. R. and Lou, M., "Low-diffusion flux-splitting methods for flows at all speeds," *AIAA J.*, pp. 1610-1617, 1998.

[47] Chorin, A. J., "A numerical method for solving incompressible viscous flow problems," *J. of Comput. Phys.*, vol. 2, pp. 12-26, 1967.

[48] Hirsch, C., Numerical Computation of Internal and External Flows, Volume 2: Computational Methods for Inviscid and Viscous Flows, John Wiley & Sons, New York, NY, 1984.

[49] Hedstrom, G. W., "Nonreflecting boundary conditions," *J. of Comput. Phys.*, vol. 30, pg. 222, 1979.

APPENDIX A CTH Time Step Modifications for Low Speed Flows

This appendix describes the time step modifications made to the CTH shock physics code for efficient time integration at low speed flows. The modifications are based on the pressure gradient scaling (PGS) technique developed by Ramshaw *et al.* [40], and are adapted for use in CTH. In this approach, the pressure gradient term (*i.e.*, normal component of the stress deviator tensor) is scaled by a constant factor when the spatial variations of the mean pressure are small. This scaling modifies the propagation speeds of acoustic disturbances to lower speeds allowing for a larger time step to be chosen for the acoustic limited CFL time step. For the shock-induced turbulent mixing problems, the spatial variations of the pressure are expected to be small after an initial short term shock event propagates out of the computational domain. After this event, the flow is dominated by advection processes for which the acoustics serve to mainly equilibrate the pressure of the system to the ambient pressure. Discussion on the implementation of PGS can be found in Ref. [40]. The following details changes to the non-reflecting boundary condition in CTH using a a one-dimensional characteristic analysis. The characteristic analysis provides information on how the eigenfunctions and eigenvalues of the hyperbolic system are changed with the introduction of the PGS. The results of this analysis are used for the calculation of the time step and modifying the non-reflecting boundary condition in CTH to be compatible with the PGS.

A.1 Characteristic Analysis using PGS for Non-reflecting Boundary Conditions

For illustration purposes, consider the system of 1-D differential equations for an ideal gas written in Cartesian coordinates conservation form,

$$\frac{\partial \vec{W}}{\partial t} + \frac{\partial \vec{F}_n}{\partial n} = \vec{C} \tag{A-1}$$

The vector quantities $\vec{W}$ and $\vec{E}$ are the conservation variables and flux vector normal to a boundary and are defined as: $\vec{W} = [\rho, \rho u, \rho v, \rho w, \rho E]^T$, $\vec{F}_n = [\rho u, \rho u^2 + p/\alpha^2, \rho uv, \rho uw, \rho uH]^T$, respectively. The variables u, v and w are the velocities associated with the normal and tangential components of velocity. The source term $\vec{C}$ accounts for the remaining fluxes tangential to the surface boundary and additional terms associated with molecular momentum and heat diffusion processes. The $1/\alpha^2$ term in front of the pressure term is a scaling term suggested by Ramshaw *et al.* [40]. In order to see the effects of this term on the eigenvalues and eigenvectors of the system, Eq. (A-1) is first expressed in terms of primitive variables, $\vec{Q} = [\rho, p, u, v, w]^T$ using the following transformation,

$$\frac{\partial \vec{Q}}{\partial t} + \underbrace{\left(\frac{\partial \vec{W}}{\partial \vec{Q}}\right)^{-1} \frac{\partial \vec{F}_n}{\partial \vec{Q}} \frac{\partial \vec{Q}}{\partial n}}_{\boldsymbol{A}} = \left(\frac{\partial \vec{W}}{\partial \vec{Q}}\right)^{-1} \vec{C} \tag{A-2}$$

where the matrices $\partial \vec{W}/\partial \vec{Q}$ and $\partial \vec{F}_n/\partial \vec{Q}$ are given as:

$$\frac{\partial \vec{W}}{\partial \vec{Q}} = \begin{bmatrix} 1 & 0 & 0 & 0 & 0 \\ H - CpT & 1/(\gamma - 1) & \rho u & \rho v & \rho w \\ u & 0 & \rho & 0 & 0 \\ v & 0 & 0 & \rho & 0 \\ w & 0 & 0 & 0 & \rho \end{bmatrix}$$

$$\frac{\partial \vec{F}_n}{\partial \vec{Q}} = \begin{bmatrix} u & 0 & 0 & 0 & 0 \\ u(H - CpT) & u\gamma/(\gamma - 1) & \rho(H + u^2) & \rho uv & \rho uw \\ u^2 & 1/\alpha^2 & 2\rho u & 0 & 0 \\ uv & 0 & \rho v & \rho u & 0 \\ uw & 0 & \rho w & 0 & \rho u \end{bmatrix} \quad \text{(A-3)}$$

The matrix $\boldsymbol{A}$ can be diagonalized as: $\boldsymbol{A} = \boldsymbol{S}\Lambda\boldsymbol{S}^{-1}$, where the rows of $\boldsymbol{S}$ are the left eigenvectors, the columns of $\boldsymbol{S}^{-1}$ are the right eigenvectors and Λ is the matrix of eigenvalues. These matrices are summarized below as follows:

$$\boldsymbol{S} = \begin{bmatrix} 0 & 0 & \frac{1}{\gamma RT} & -\frac{\alpha(u' - c') + [\gamma(1 - \alpha^2) - 1]u}{2\alpha^2 c^2 c'} & \frac{\alpha(u' + c') + [\gamma(1 - \alpha^2) - 1]u}{2\alpha^2 c^2 c'} \\ 0 & 0 & 0 & -\frac{u' - c' - u}{2c'} & \frac{u' + c' - u}{2c'} \\ 0 & 0 & 0 & -\frac{1}{2\alpha^2 \rho c'} & \frac{1}{2\alpha^2 \rho c'} \\ 0 & 1 & 0 & 0 & 0 \\ 1 & 0 & 0 & 0 & 0 \end{bmatrix} \quad \text{(A-4)}$$

$$\boldsymbol{S}^{-1} = \begin{bmatrix} 0 & 0 & 0 & 0 & 1 \\ 0 & 0 & 0 & 1 & 0 \\ \gamma(\gamma - 1)T & -1 & (\alpha^2 - 1)(\gamma - 1)\rho u & 0 & 0 \\ 0 & 1 & \rho\alpha^2(u - u' - c') & 0 & 0 \\ 0 & 1 & \rho\alpha^2(u - u' + c') & 0 & 0 \end{bmatrix} \qquad \Lambda = \begin{bmatrix} u & 0 & 0 & 0 & 0 \\ 0 & u & 0 & 0 & 0 \\ 0 & 0 & u & 0 & 0 \\ 0 & 0 & 0 & u' - c' & 0 \\ 0 & 0 & 0 & 0 & u' + c' \end{bmatrix}$$

where $u' + c'$ and $u' - c'$ are the modified eigenvalues of the system associated with the propagation of acoustic information and are defined as follows.

$$u' = \frac{u}{2}[\gamma(1 - 1/\alpha^2) + (1/\alpha^2 + 1)]$$
$$c' = \frac{c}{2}\sqrt{(\gamma - 1)^2 M^2 (1 - 1/\alpha^2)^2 + 4/\alpha^2} \quad \text{(A-5)}$$

Inspection of Eq. (A-5) reveals that in the limit as $\alpha \to 1$ both u' and c' approach the non-preconditioned values of u and c, respectively. Also, it is interesting to see the similarities of the

eigenvalues of preconditioned system using the PGS of Eq. (A-5) and more recent work on the state-of-the-art preconditioning algorithms for the compressible Navier Stokes equations [44-46]. The eigenvalues of those systems strongly resemble Eq. (A-5) indicating that the same hyperbolic system of equations are solved in each case. However, in the preconditioned systems of Refs. [44-46] a subcycling procedure is employed for every physical time step for which the pseudo-acoustics of the system are allowed to propagate out of the domain before the next physical time step. This subcyling is not employed using PGS where pseudo-acoustic waves are allowed to propagate around in the domain on the time scales as the mean advection processes. It is expected that the differences between these two approaches will be small for flows for which the pressure changes in the computational domain are small, consistent with the underlying assumptions for using the PGS technique.

Multiplying Eq. (A-2) through by $\boldsymbol{S}^{-1}$, and for the moment ignoring the source term on the right hand side, transforms this equation into the following characteristic form,

$$\frac{\partial \vec{\Re}}{\partial t} + \Lambda \frac{\partial \vec{\Re}}{\partial n} = 0 \tag{A-6}$$

where $\delta\vec{\Re} = \boldsymbol{S}^{-1}\delta\vec{Q}$ are defined as the Riemann invariants [48] and explicitly identify the direction for which information propagates. These terms are given below as:

$$\delta\vec{\Re} = \begin{bmatrix} \delta\Re_1 \\ \delta\Re_2 \\ \delta\Re_3 \\ \delta\Re_4 \\ \delta\Re_5 \end{bmatrix} = \begin{bmatrix} u\delta w \\ u\delta v \\ c^2\delta\rho - 2\alpha^2\rho(u-u')\delta u - \delta p \\ \delta p + \alpha^2\rho\delta u(u-u'-c') \\ \delta p + \alpha^2\rho\delta u(u-u'+c') \end{bmatrix} \tag{A-7}$$

and represent the wave amplitudes of information coming into and out of the computational domain. The invariants are and their speed of propagation using PGS are sketched below for $u > 0$ on a right boundary.

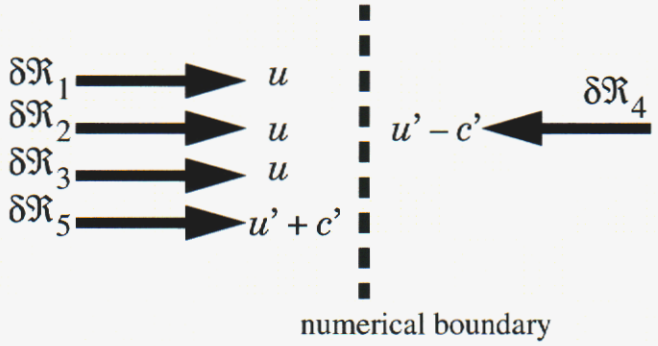

Figure A-1: Sketch of Riemann invariants at boundary of computational domain for $u > 0$.

In CTH the Riemann invariants associated with information leaving the domain is simply calculated using an upwinded difference as part of the Lagrangian time step. The invariant associated with information coming into the domain is determined using the non-reflecting boundary condition of Hedstrom [49] which states that the time rate of change of the wave amplitude coming into the domain is equal to zero,

$$\frac{\partial \Re_4}{\partial t} = 0 \tag{A-8}$$

or using the definition of $\Re_4$,

$$\rho(u' - u + c')\frac{\partial u}{\partial t} = \frac{1}{\alpha^2}\frac{\partial p}{\partial t}. \tag{A-9}$$

Previously, McGlaun [37] generalized the boundary condition of Hedstrom for use with CTH into a statement for the normal stress, σ_n, component on the boundary condition,

$$\rho c\frac{\partial u}{\partial t} = \frac{\partial \sigma_n}{\partial t} \tag{A-10}$$

which after numerous algebraic manipulations (details in ref. [37]) results in the following expression to update the normal stress on the boundary of the computational domain at the $t + \Delta t/2$ time level.

$$\overline{\sigma}_n^{(t+\Delta t/2)} = \frac{\Delta z}{\Delta z + c\Delta t}\left\{\overline{\sigma}_n^{(t-\Delta t/2)} + \frac{c\Delta t\ \sigma_n^{\,t}}{\Delta z} + \frac{c\overline{\Delta t}}{\Delta z}(\sigma_n^{\,t} - \overline{\sigma}_n^{(t-\Delta t)}) - \frac{c(\Delta t + \overline{\Delta t})}{2}\xi^t\right\} \tag{A-11}$$

In Eq. (A-11), σ_n and $\overline{\sigma_n}$ are the normal stress components at the node and at the cell interface between the last node and the ghost cell, respectively, as shown in the below sketch,

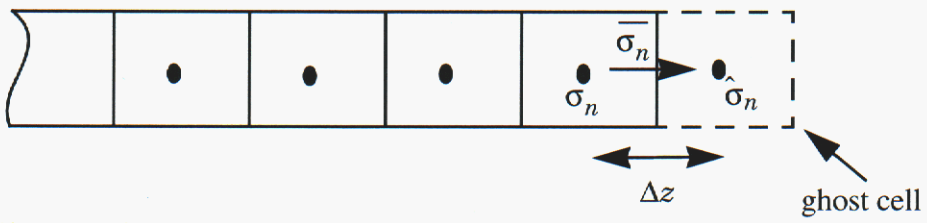

Figure A-2: Definition of cell normal stresses in CTH near boundaries.

and ξ^t represents the rest of the stress deviators and any additional source terms in the momentum transport equation. The non-reflecting boundary condition is re-derived using an equivalent expression to Eq. (A-10) for use with PGS based on Eq. (A-9),

$$\rho(u' - u + c')\frac{\partial u}{\partial t} = \frac{1}{\alpha^2}\frac{\partial \sigma_n}{\partial t} \tag{A-12}$$

resulting in the following for the updated stress on the boundary,

$$\overline{\sigma}_n^{(t+\Delta t/2)} = \frac{\Delta z}{\Delta z + \Delta t(c/\alpha)}\left\{\overline{\sigma}_n^{(t-\Delta t/2)} + \frac{c\Delta t\ \sigma_n{}^t}{\alpha\Delta z} + \frac{c\overline{\Delta t}}{\alpha\Delta z}(\sigma_n{}^t - \overline{\sigma}_n^{(t-\Delta t)}) - \frac{\alpha c(\Delta t + \overline{\Delta t})}{2}\xi^t\right\}. \quad \text{(A-13)}$$

Note, the difference between Eq. (A-11) and Eq. (A-13) is the re-scaling of the speed of sound by the α parameter for all terms except the last where the source term is multiplied by the α.

A.2 Assessment of PGS Non-reflecting Boundary Condition

A simple convection problem is used as a test of the modified boundary condition for use with the pressure gradient scaling. Figure A-3 shows the setup of the problem and consists of a round blob of material at an initial velocity and density of 10 m/s and 0.002 g/cc, respectively. The blob is set in a lower density fluid of 0.001 g/cc. Three cases using PGS are run to examine changes to the non-reflecting boundary condition. The first case uses a 100 cm x 100 cm computational domain that is much larger than the domain shown in Fig. A-3 and the simulation is stopped before any pseudo-acoustic disturbance reaches the boundary. This case can then be thought as the exact solution to using a non-reflecting boundary condition for the finite 17.5 cm x 17.5 cm domain of Fig. A-3. Figures A-4 (a) and (b) show material and pressure contours early in the simulation after 7.5 ms. At this time, the pseudo-acoustic wave front has propagated approximately 20 cm. A finite 17.5 cm x 17.5 cm computational domain is used in case 2. Figures A-5 (a) and (b) show results from this case when without any modifications to original CTH non-reflecting boundary condition. As shown in the pressure contour, waves are reflected back into the domain indicating that the boundary exhibits an effective acoustic impedance for the pseudo-acoustic waves. In the third case, the non-reflecting boundary condition of Eq. (A-13) is used and run for the same conditions as case 2. Figures A-6 (a) and (b) show that, with the modifications, the acoustic disturbance propagates out of the domain with no reflection from the boundaries. Lastly, pressure and material and pressure contours are presented in Figs. A-7 (a) and (b) for case 2 at a much later time. Large fluctuations in pressure are observed along the lower boundary and, for some cases, numerical instabilities will result if the original non-reflecting boundary condition is used with the PGS.

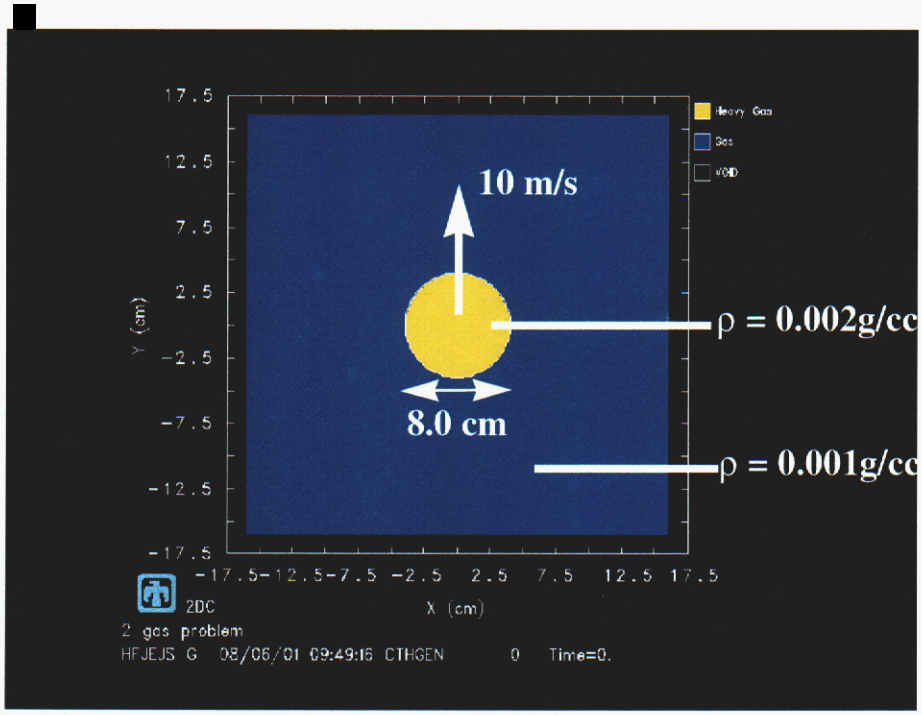

Figure A-3: Initial conditions for convection problem using PGS.

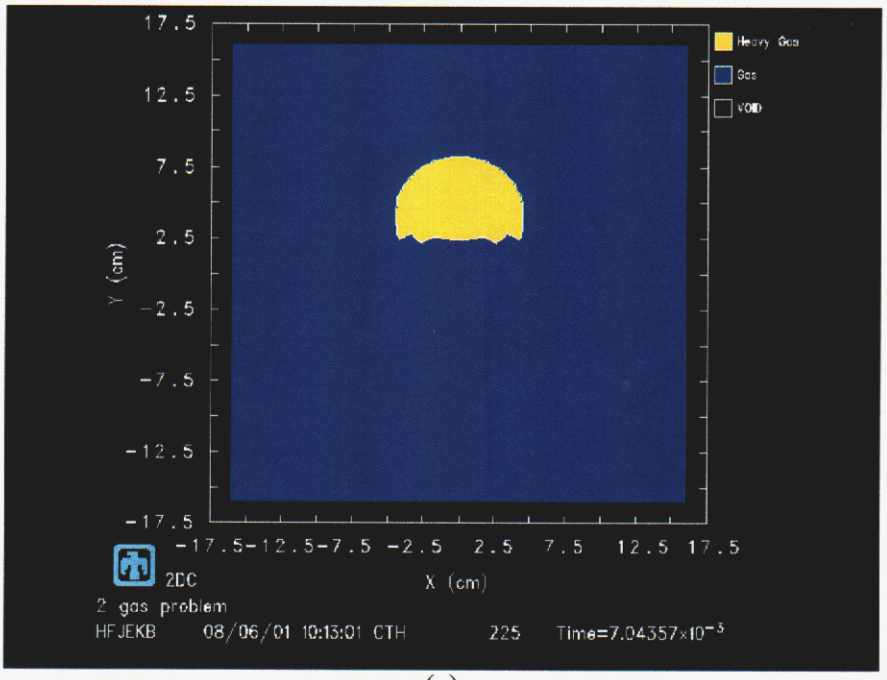

(a)

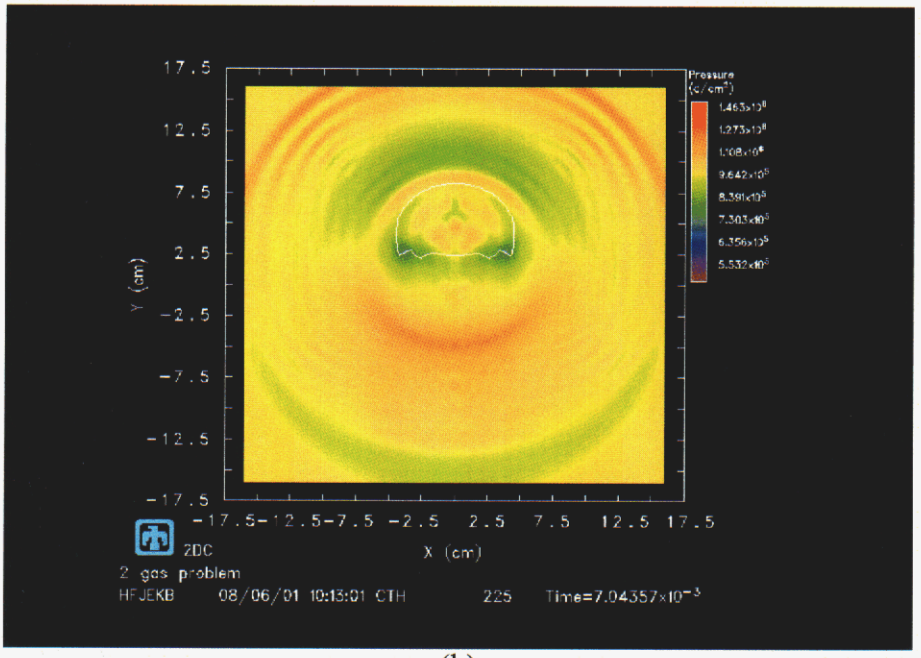

(b)

Figure A-4: Contour plots of (a) material and (b) pressure distributions early in time using a large computational domain, representing the exact solution.

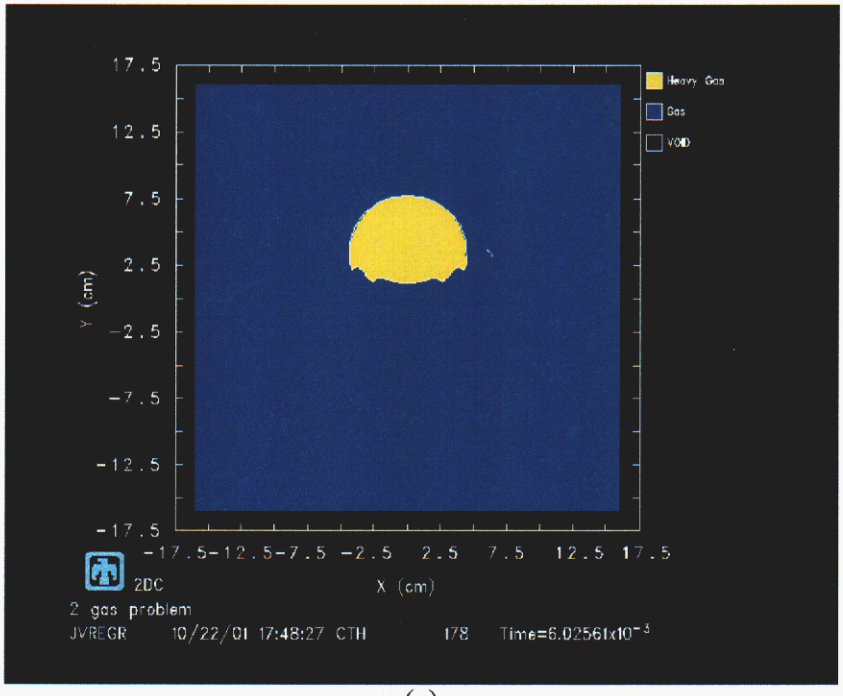

(a)

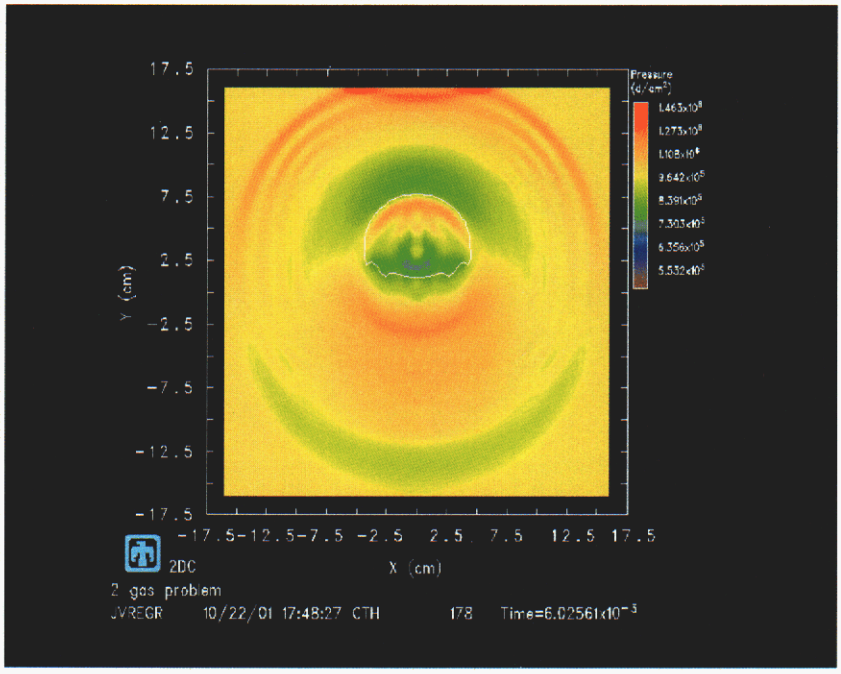

(b)

Figure A-5: Contour plots of (a) material and (b) pressure distributions early in time using the original CTH non-reflecting boundary condition.

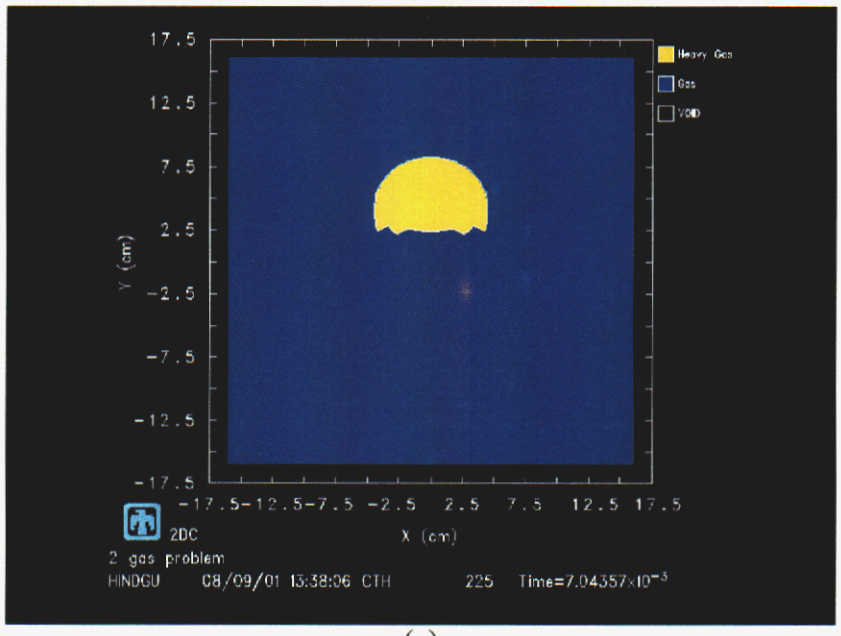

(a)

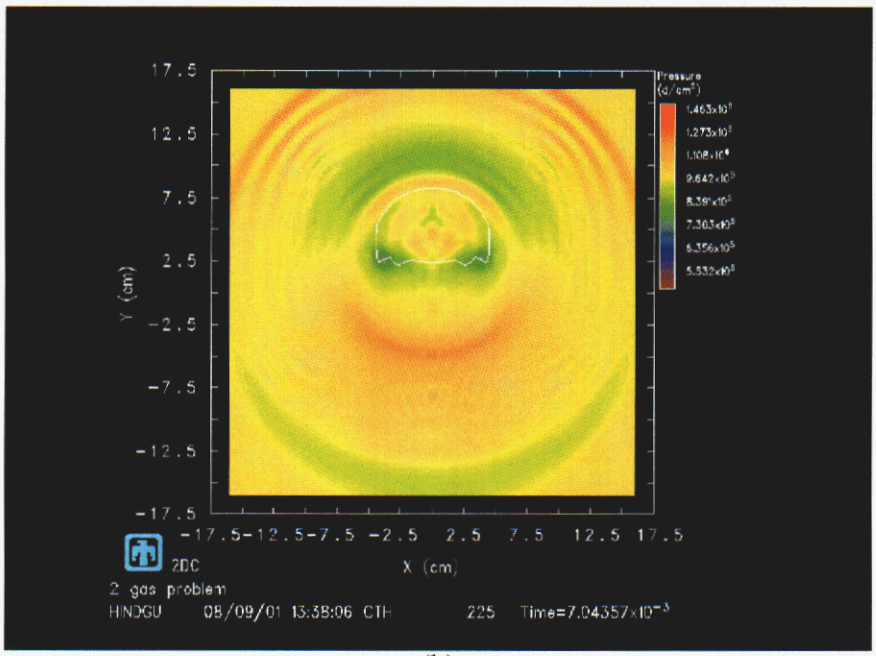

(b)

Figure A-6: Contour plots of (a) material and (b) pressure distributions early in time using the PGS modified CTH non-reflecting boundary condition.

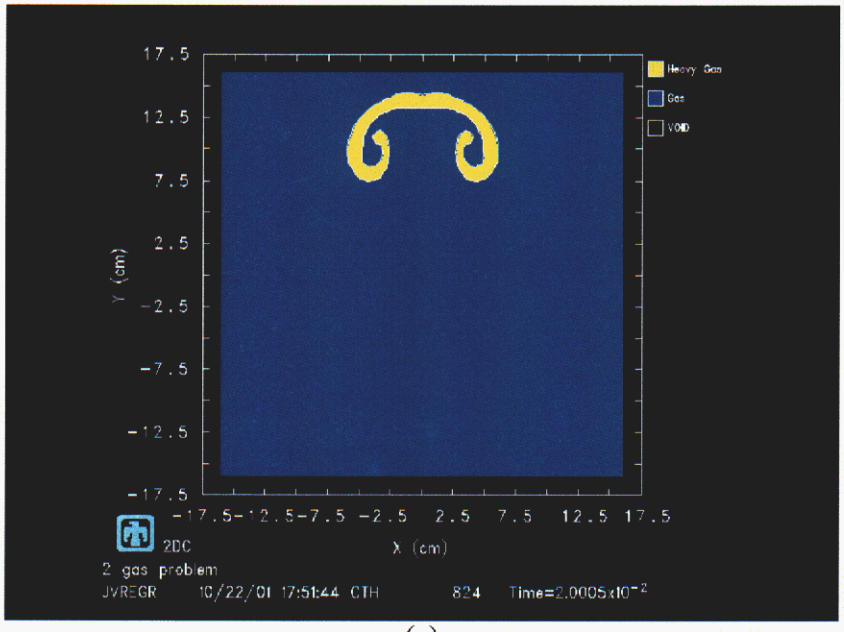

(a)

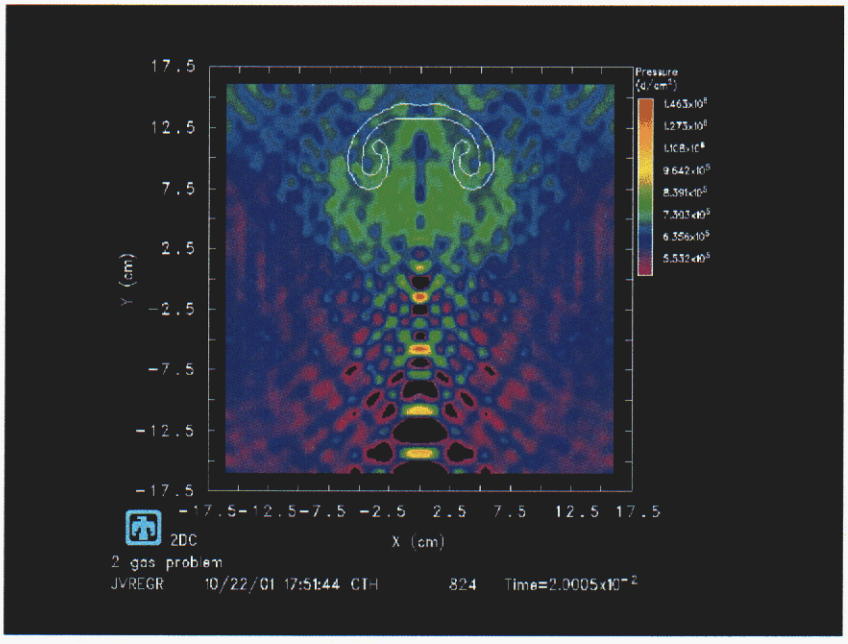

(b)

Figure A-7: Contour plots of (a) material and (b) pressure distributions late in time using the original CTH non-reflecting boundary.

Distribution

1	MS 0824	J. L. Moya, 9130
1	MS 0824	A. C. Ratzel, 9110
1	MS 0835	S. N. Kempka, 9141
1	MS 0835	S. P. Domino, 9141
5	MS 0836	M. R. Baer, 9100
1	MS 0836	D. A. Crawford, 9116
1	MS 0836	L. J. DeChant, 9116
5	MS 0836	E. S. Hertel, 9116
1	MS 0893	R. M. Brannon, 9123
1	MS 0821	L. A. Gritzo, 9132
10	MS 0836	P. E. DesJardin, 9132
1	MS 0836	S. R. Tieszen, 9132
1	MS 0841	T. C. Bickel, 9100
1	MS 0835	J. M. McGlaun, 9140
1	MS 0819	S. P. Burns, 9231
5	MS 0820	R. L. Bell, 9232
1	MS 0820	M. E. Kipp, 9232
1	MS 0820	P. A. Taylor, 9232
1	MS 0316	T. M. Smith, 9233
1	MS 1454	A. M. Renlund, 2554
1	MS 9051	J. C. Oefelein, 8351
1	MS 9051	A. R. Kerstein, 8351

Leonard Wilson
Naval Surface Warfare Center
Dalhlgren Division, Code G22
Dahlgren, VA 22448-5000

Michael Hopson
Naval Surface Warfare Center
Dahlgren Division, Code G22
Dahlgren VA 22448-5000

Robert Garrett
Naval Surface Warfare Center
Dahlgren Division, Code G24
Dahlgren VA 22448-5000

Kibong Kim
DTRA
6801 Telegraph Road
Alexandria, VA 22310

1	MS 9018	Central Technical Files, 8945-1
2	MS 0899	Technical Library, 9616
1	MS 0612	Review and Approval desk, 9612, For DOE/OSTI